Hybrid uncertainty propagation based on multi-fidelity surrogate model

Jinxing Liu[a], Yan Shi[a,*], Chen Ding[a], Michael Beer[a,b,c]

[a]*Institute for Risk and Reliability, Leibniz Universität Hannover, Hannover 30167, Germany*
[b]*Institute for Risk and Uncertainty, University of Liverpool, Liverpool L69 7ZF, United Kingdom*
[c]*International Joint Research Center for Resilient Infrastructure & International Joint Research Center for Engineering Reliability and Stochastic Mechanics, Tongji University, Shanghai 200092, China*

Abstract

There always exist multiple uncertainties including random uncertainty, interval uncertainty, and fuzzy uncertainty in engineering structures. In the presence of hybrid uncertainties, the hybrid uncertainty propagation analysis can be a challenging problem, which suffers from the computational burden of double-loop procedure when numerical simulation techniques are employed. In this work, a novel method for efficient hybrid uncertainty propagation analysis with the three types of uncertainties is proposed. Generally, multi-fidelity surrogate models, such as Co-Kriging, can greatly improve the computational efficiency by leveraging information from a low-fidelity model to build a high-fidelity approximate model. However, the traditional multi-fidelity surrogate model methods always calculate the hybrid uncertainty propagation result by combining with several numerical simulation techniques. This process can introduce post-processing errors unless unlimited number of samples are used, which is impossible in engineering application. In order to address this issue, the analytical solutions of the output mean and output variance are derived based on the Co-Kriging, and the resulting mean and variance are both random variables. Moreover, a new adaptive framework is established to strengthen the estimation accuracy of the hybrid uncertainty propagation result, by combining the augmented expected improvement function and the derived mean random variable. Several applications are introduced to demonstrate the effectiveness of the proposed method for solving hybrid uncertainty propagation problems.

Keywords: Hybrid uncertainties; Uncertainty propagation; Multi-fidelity surrogate model; Analytical solution; Adaptive framework

*Corresponding author
Email address: yan.shi@irz.uni-hannover.de (Yan Shi)

1. Introduction

Uncertainty is pervasive in engineering practice due to the inevitable variability of structures. These uncertainties in inputs can have a significant impact on responses of interest. Thus, uncertainty propagation analysis, which aims to quantify the uncertainties in the output that propagate from the input, has become a crucial foundation of uncertainty quantification, such as reliability-based design optimization (RBDO) [1, 2] and robust design optimization (RDO) [3, 4]. However, how to assess this propagation of uncertainty remains a challenge due to the increasing complexity of engineering structures. To this end, many uncertainty propagation approaches have been investigated, including simulation-based methods [5, 6], Taylor series expansion-based methods [7, 8], numerical integration-based method [9, 10], and surrogate model-based methods [11, 12], etc.

Generally, the notion of uncertainty can be divided into two distinct classes: aleatory and epistemic uncertainties [13, 14]. Aleatory uncertainty, also termed as inherent uncertainty, describes the natural randomness of structural system. This type of uncertainty is irreducible and it is usually handled by probabilistic methods. Epistemic uncertainty, on the other hand, stems from scarce experimental data or insufficient information. As more knowledge or samples become available, this type of uncertainty can be reduced. For aleatory uncertainty, random variables with precise probability distributions are used to characterize input uncertainties. For epistemic uncertainty, because available information is imprecise, evidence theory (also known as Dempster–Shafer theory), fuzzy set theory, interval theory, etc., are usually adopted to represent input parameters.

Monte Carlo simulation (MCS) [15] is a traditional simulation-based method, the results of which are widely used as a reference to verify the accuracy of other methods due to its simplicity and robustness. However, for MCS, as well as some improved simulation-based methods (e.g., subset simulation (SS), importance sampling (IS), directional simulation (DS), line sampling (LS), etc.), the prohibitive computational cost is still a limitation, especially when a single simulation is time-consuming and multiple uncertainties coexist. Over the past few decades, some research has been done on uncertainty propagation problems involving only one type of uncertainty. For example, Rao and Berke [16] applied interval analysis to uncertain structures. Lee and Chen [17] performed a comparative study on the performances of some uncertainty propagation methods. In the work of Wei et al. [18], polynomial chaos expansion constructed with points of monomial cubature rules is proposed for uncertainty propagation. Long et al. [19] presented an interval analysis method for the fatigue crack growth life prediction. Liu et al. [20] provided a non-probabilistic uncertainty propagation method, where the uncertain parameters are modeled using the ellipsoidal convex set. Wang and Matthies [21] proposed a modified parallelepiped model for the non-probabilistic uncertainty propagation. Remarkably, one of the most common scenarios in engineering is where the two uncertainties mentioned above exist simultaneously. Therefore, the development of practical methods for hybrid uncertainty propagation analysis needs to be focused. Jiang et al. [22] reviewed four main research directions in probability-interval hybrid uncertainty analysis. Pedroni et al. [23] applied the joint hierarchical propagation of hybrid uncertainty to a model for the risk-based design of a flood protection dike. In the work of Wang and Matthies [24–26], some uncertain models and numerical computing methods were presented for hybrid uncertainty propagation analysis. Dang et al. [27] developed a Bayesian framework for propagating hybrid uncertainties. Long et al. [28] presented a unified framework to address the hybrid uncertainty problems under four types of uncertainties, i.e., probabilistic, evidence, fuzzy and interval uncertainties. Despite the significant progress mentioned above, research on hybrid uncertainty analysis methods is still at a preliminary stage, and most research considers only two types of uncertainties. Due to the increasing complexity of structures, efficient methods that can accommodate more than two types of uncertainties for hybrid uncertainty analysis are desirable.

Although the surrogate model is widely used in uncertainty analysis, the computational burden of constructing a surrogate model can still be heavy when a single simulation is extremely time-consuming. Furthermore, even resorting to surrogate model, hybrid uncertainty propagation is still generally performed using numerical methods, which inevitably introduce post-processing errors. To avoid the post-processing errors, Shi et al. [29] derived the analytical solutions of the output mean and variance based on the Kriging model for RDO. Chen et al. [30] proposed an adaptive method for uncertainty analysis based on the Kriging model associated with analytical solutions of the output mean and variance. However, the above methods are not applicable to uncertainty propagation for multi-fidelity models, and the above methods cannot deal with hybrid uncertainty problems. Co-Kriging [31, 32], as a typical multi-fidelity surrogate model, can make a good trade-off between accuracy and efficiency. Based on the Co-Kriging model, this paper aims to develop a fully decoupled adaptive method for hybrid uncertainty propagation analysis involving three types of uncertainties, i.e., random, interval and fuzzy variables. The novelty of this study can be summarized as follows. First, based on the Co-Kriging model, the analytical solutions for the output mean and the output variance are derived, which can be computed efficiently without additional simulation. These analytical solutions are still random variables, and are explicit functions with respect to epistemic variables. Second, a new adaptive framework for hybrid uncertainty propagation is established in which the variance of the output mean is also analytically derived to measure the modeling uncertainty and enable active learning. In this framework, update samples are determined sequentially for high-fidelity (HF) and low-fidelity (LF) simulation. Third, two new convergence criteria are designed to terminate the adaptive process when a desired level of accuracy for the bounds on the output mean and the output variance is achieved. To the best of our knowledge, these analytical solutions have not been derived before. The proposed method requires only a few samples to compute the analytical solutions of the output mean and output variance, and can avoid the post-processing errors in hybrid uncertainty propagation analysis.

The outline of this paper is as follows. Section 2 provides a detailed formulation of the problem considered in this paper. Then, a fully decoupled adaptive method for hybrid uncertainty propagation analysis is presented in Section 3. Four case studies are investigated in Section 4 to demonstrate the effectiveness and efficiency of the proposed method. Finally, the conclusions are given in Section 5.

2. Formulation of the problem

In traditional uncertainty propagation analysis, only random variables are employed to measure the input uncertainty of structures. Nonetheless, when hybrid uncertainties are present in structures, the uncertainty analysis becomes more complicated. In this study, we address the hybrid uncertainty propagation with the coexistence of three distinct types of input uncertainties, namely, random, interval, and fuzzy variables.

2.1. Interval and fuzzy variables

Generally, a large number of samples is required to obtain the exact probability distribution of the input parameter, but in practice this is difficult to achieve due to the huge computational or economic burden. In fact, closed intervals (i.e., the range of variation), which are easier to obtain, are often used to represent uncertain parameters in many cases. Remarkably, there is no assumption of probability distribution for interval variables, of which the bounds are determined based on engineering experience. The interval variable Y is defined as follows [33]:

$$Y \in [Y^L, Y^U], \quad Y^m = \frac{Y^L + Y^U}{2}, \quad Y^r = \frac{Y^U - Y^L}{2} \tag{1}$$

where Y^L, Y^U, Y^m and Y^r denote the lower bound, the upper bound, the midpoint, and the radius of Y, respectively.

Fuzzy variables are related to fuzzy sets which are first introduced by Zadeh [34]. Let Z be a fuzzy variable, which is a set mathematically defined by the following pair:

$$Z = \{\langle z,\ m(z)\rangle |\, z \in \Omega,\ m(z) \in [0,1]\} \tag{2}$$

where z is the general elements of the fuzzy set, Ω is the definition domain of the fuzzy set, and $m(z) : \Omega \to [0,1]$ is the membership function. It should be noted that the value of $m(z)$ represents the membership degree of z in the fuzzy set. In other words, it represents the degree of possibility that the fuzzy variable takes the value of z. $m(z) = 0$ means that element z is not included in the fuzzy set, while $m(z) = 1$ means that element z is fully included in the fuzzy set. $m(z)$ between 0 and 1 means that element z is partially included in the fuzzy set.

The α-cut approach plays an important role in the implementation of fuzzy arithmetic. Given a cut level α, the α-cut of a fuzzy set can be denoted as [35]:

$$Z_\alpha = \{z \mid m(z) \geq \alpha, z \in \Omega, 0 \leq \alpha \leq 1\} \tag{3}$$

which is a set consisting of the elements z whose membership values $m(z)$ are equal to or greater than the cut level α. For a certain cut level α, the corresponding set Z_α can be regarded as an interval variable Z_α^I:

$$Z_\alpha^I = [Z_\alpha^L, Z_\alpha^U] = \left\{z \in \Omega \mid Z_\alpha^L \leq z \leq Z_\alpha^U\right\} \tag{4}$$

where Z_α^L and Z_α^U represent the lower and upper bounds of Z_α^I, respectively. There are various types of membership functions that define distinct forms of fuzzy variables, and the triangular membership function is used in this paper. The triangular membership function is described by piecewise linear segments:

$$m(z) = \begin{cases} \dfrac{z-a}{b-a} & \text{if } a \leq z \leq b \\ \dfrac{c-z}{c-b} & \text{if } b \leq z \leq c \\ 0 & \text{otherwise} \end{cases} \tag{5}$$

Intuitively, Fig. 1 shows a triangular membership function and the α-cut interval Z_α^I. In this context, fuzzy sets can be seen as a generalization of interval variables, and both of them are usually used to describe epistemic uncertainty.

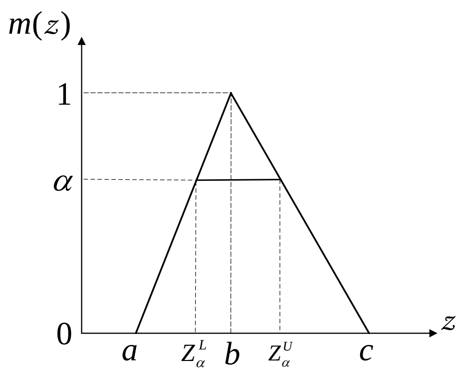

Figure 1: Diagram of the triangular membership function of fuzzy variable Z

2.2. Statement of hybrid uncertainty propagation analysis

For a hybrid uncertainty problem, there are multiple types of variables, and the relationship between the input parameters and the response of interest can be described by the performance function g:

$$G = g(\boldsymbol{X}, \boldsymbol{Y}, \boldsymbol{Z}) \tag{6}$$

where G denotes the response of interest, $\boldsymbol{X} = [X_1, X_2, ..., X_{n_{\boldsymbol{X}}}]^{\mathrm{T}}$ is the $n_{\boldsymbol{X}}$-dimensional input vector of random variables, $\boldsymbol{Y} = [Y_1, Y_2, ..., Y_{n_{\boldsymbol{Y}}}]^{\mathrm{T}}$ denotes the $n_{\boldsymbol{Y}}$-dimensional input vector of interval variables, and $\boldsymbol{Z} = [Z_1, Z_2, ..., Z_{n_{\boldsymbol{Z}}}]^{\mathrm{T}}$ denotes the $n_{\boldsymbol{Z}}$-dimensional input vector of fuzzy variables. In this setting, the uncertainties in the inputs are propagated to the response G, which is also a random variable under arbitrary values of interval and fuzzy variables. In engineering practice, it is usually difficult to obtain the exact probability density function (PDF) of the response because the input random variables may follow different types of distributions and the performance function is often nonlinear.

In this study, the primary objective is to assess the effect of uncertainties in the inputs on the response G through the analytical expressions of the output mean $u_g(\boldsymbol{y}, \boldsymbol{z})$ and the output variance $\sigma_g^2(\boldsymbol{y}, \boldsymbol{z})$, which are functions of the values of interval and fuzzy variables:

$$u_g(\boldsymbol{y}, \boldsymbol{z}) = \int_{\Omega_{\boldsymbol{X}}} g(\boldsymbol{x}, \boldsymbol{y}, \boldsymbol{z}) f_{\boldsymbol{X}}(\boldsymbol{x}) \mathrm{d}\boldsymbol{x} \tag{7}$$

$$\sigma_g^2(\boldsymbol{y}, \boldsymbol{z}) = \int_{\Omega_{\boldsymbol{X}}} [g(\boldsymbol{x}, \boldsymbol{y}, \boldsymbol{z}) - u_g(\boldsymbol{y}, \boldsymbol{z})]^2 f_{\boldsymbol{X}}(\boldsymbol{x}) \mathrm{d}\boldsymbol{x} \tag{8}$$

where $f_{\boldsymbol{X}}(\boldsymbol{x})$ is the joint PDF, $\Omega_{\boldsymbol{X}}$ denotes the value domain of $\boldsymbol{X}$, and $\boldsymbol{x}$, $\boldsymbol{y}$, $\boldsymbol{z}$ are the realization of $\boldsymbol{X}$, $\boldsymbol{Y}$, $\boldsymbol{Z}$, respectively. Furthermore, due to the presence of interval and fuzzy variables, the output mean $u_g(\boldsymbol{y}, \boldsymbol{z})$ and the output variance $\sigma_g^2(\boldsymbol{y}, \boldsymbol{z})$ are no longer crisp values, but intervals at each cut level α.

3. The proposed method

3.1. Performance approximation with Co-Kriging

As an extension of Kriging, Co-Kriging has attracted a great deal of attention in the field of engineering [36, 37]. It is an multi-fidelity surrogate model that combines the HF and LF models to provide a trade-off between accuracy and efficiency. The conventional single-fidelity Kriging model requires that all samples are from the HF model, where computational burden is still a limitation when the simulation is extremely time-consuming. In this regard, Co-Kriging uses a limited number of expensive HF samples and more relatively cheap LF samples to construct an multi-fidelity model. Denote the model input as $\boldsymbol{\xi}$, and the Co-Kriging prediction can be expressed as [38]:

$$S_{\mathrm{e}}(\boldsymbol{\xi}) = \rho S_{\mathrm{c}}(\boldsymbol{\xi}) + S_{\mathrm{d}}(\boldsymbol{\xi}) \tag{9}$$

where $S_{\mathrm{c}}(\boldsymbol{\xi})$ denotes the LF Kriging prediction, $S_{\mathrm{d}}(\boldsymbol{x})$ denotes Kriging model of the difference between HF and LF model predictions, and ρ is a scaling factor. Let $\boldsymbol{D}_{\mathrm{c}} = (\boldsymbol{\xi}_{\mathrm{c}}^{(1)}, \boldsymbol{\xi}_{\mathrm{c}}^{(2)}, ..., \boldsymbol{\xi}_{\mathrm{c}}^{(n_{\mathrm{c}})})^{\mathrm{T}}$ denote an n_{c}-by-n matrix consisting of n_{c} LF samples whose responses are $\boldsymbol{y}_{\mathrm{c}} = (y_{\mathrm{c}}^{(1)}, y_{\mathrm{c}}^{(2)}, ..., y_{\mathrm{c}}^{(n_{\mathrm{c}})})^{\mathrm{T}}$, $\boldsymbol{D}_{\mathrm{e}} = (\boldsymbol{\xi}_{\mathrm{e}}^{(1)}, \boldsymbol{\xi}_{\mathrm{e}}^{(2)}, ..., \boldsymbol{\xi}_{\mathrm{e}}^{(n_{\mathrm{e}})})^{\mathrm{T}}$ denote an n_{e}-by-n matrix consisting of n_{e} HF samples whose responses are $\boldsymbol{y}_{\mathrm{e}} = (y_{\mathrm{e}}^{(1)}, y_{\mathrm{e}}^{(2)}, ..., y_{\mathrm{e}}^{(n_{\mathrm{e}})})^{\mathrm{T}}$, and n is the dimension of the sample points. The covariance matrix of Co-Kriging is expressed in block form as:

$$\boldsymbol{C} = \begin{bmatrix} \sigma_{\mathrm{c}}^2 \boldsymbol{\Psi}_{\mathrm{c}}(\boldsymbol{D}_{\mathrm{c}}, \boldsymbol{D}_{\mathrm{c}}) & \rho\sigma_{\mathrm{c}}^2 \boldsymbol{\Psi}_{\mathrm{c}}(\boldsymbol{D}_{\mathrm{c}}, \boldsymbol{D}_{\mathrm{e}}) \\ \rho\sigma_{\mathrm{c}}^2 \boldsymbol{\Psi}_{\mathrm{c}}(\boldsymbol{D}_{\mathrm{e}}, \boldsymbol{D}_{\mathrm{c}}) & \rho^2\sigma_{\mathrm{c}}^2 \boldsymbol{\Psi}_{\mathrm{c}}(\boldsymbol{D}_{\mathrm{e}}, \boldsymbol{D}_{\mathrm{e}}) + \sigma_{\mathrm{d}}^2 \boldsymbol{\Psi}_{\mathrm{d}}(\boldsymbol{D}_{\mathrm{e}}, \boldsymbol{D}_{\mathrm{e}}) \end{bmatrix} \tag{10}$$

where σ_{c}^2 and σ_{d}^2 are the process variances of the LF and HF Kriging models, respectively, $\boldsymbol{\Psi}_{\mathrm{c}}$ and $\boldsymbol{\Psi}_{\mathrm{d}}$ are the correlation matrix of LF and HF Kriging models, respectively. Based on the LF Kriging model constructed from $\boldsymbol{D}_{\mathrm{c}}$ and $\boldsymbol{y}_{\mathrm{c}}$, σ_{c}^2 and $\boldsymbol{\Psi}_{\mathrm{c}}$ can be obtained by the maximum likelihood estimation (MLE), while σ_{d}^2 and $\boldsymbol{\Psi}_{\mathrm{d}}$ are obtained based on the difference Kriging model. To this end, the difference $\boldsymbol{d}$ is defined as:

$$\boldsymbol{d} = \boldsymbol{y}_{\mathrm{e}} - \rho \boldsymbol{y}_{\mathrm{c}}(\boldsymbol{D}_{\mathrm{e}}) \tag{11}$$

where $\boldsymbol{y}_{\mathrm{c}}(\boldsymbol{D}_{\mathrm{e}})$ denotes the responses of LF model at samples $\boldsymbol{D}_{\mathrm{e}}$. Then, σ_{d}^2 and $\boldsymbol{\Psi}_{\mathrm{d}}$ can be determined based on the difference Kriging model constructed from $\boldsymbol{D}_{\mathrm{e}}$ and $\boldsymbol{d}$.

After all parameters are estimated, at an arbitrary unknown point $\boldsymbol{\xi}$, the prediction of Co-Kriging is available, which is a random variable. The mean value can be expressed as follows:

$$\hat{y}_{\mathrm{e}}(\boldsymbol{\xi}) = \hat{\mu} + \boldsymbol{c}_{(\boldsymbol{\xi})}^{\mathrm{T}} \boldsymbol{C}^{-1} (\boldsymbol{y}^* - \mathbf{1}\hat{\mu}) \tag{12}$$

where

$$\hat{\mu} = \frac{\mathbf{1}^{\mathrm{T}}\boldsymbol{C}^{-1}\boldsymbol{y}^*}{\mathbf{1}^{\mathrm{T}}\boldsymbol{C}^{-1}\mathbf{1}} \tag{13}$$

$$\boldsymbol{c}_{(\boldsymbol{\xi})} = \begin{bmatrix} \rho\sigma_{\mathrm{c}}^2 \boldsymbol{\psi}_{\mathrm{c}}(\boldsymbol{D}_{\mathrm{c}}, \boldsymbol{\xi}) \\ \rho^2\sigma_{\mathrm{c}}^2 \boldsymbol{\psi}_{\mathrm{c}}(\boldsymbol{D}_{\mathrm{e}}, \boldsymbol{\xi}) + \sigma_{\mathrm{d}}^2 \boldsymbol{\psi}_{\mathrm{d}}(\boldsymbol{D}_{\mathrm{e}}, \boldsymbol{\xi}) \end{bmatrix} \tag{14}$$

$\boldsymbol{y}^* = [\boldsymbol{y}_{\mathrm{c}}^{\mathrm{T}}, \boldsymbol{y}_{\mathrm{e}}^{\mathrm{T}}]^{\mathrm{T}}$ is the response vector of LF and HF samples, and $\boldsymbol{\psi}$ refers to a column vector of correlations between samples and $\boldsymbol{\xi}$. Note that the subscripts $\langle \mathrm{c} \rangle$, $\langle \mathrm{e} \rangle$ and $\langle \mathrm{d} \rangle$ in this paper indicate whether the parameters used are from the LF, HF, or difference Kriging models, respectively. The variance of the prediction is expressed as:

$$s_{\mathrm{e}}^2(\boldsymbol{\xi}) = \rho^2\sigma_{\mathrm{c}}^2 + \sigma_{\mathrm{d}}^2 - \boldsymbol{c}_{(\boldsymbol{\xi})}^{\mathrm{T}} \boldsymbol{C}^{-1} \boldsymbol{c}_{(\boldsymbol{\xi})} \tag{15}$$

The reader can refer to [31] for more details about the derivation. In this study, the Gaussian correlation function shown below is used:

$$\psi_\theta\left(\boldsymbol{\xi}, \boldsymbol{\xi}'\right) = \exp\left\{-\sum_{k=1}^{n} \theta^{(k)} \left(\xi^{(k)} - \xi'^{(k)}\right)^2\right\} \tag{16}$$

where $\theta^{(k)}$ $(k = 1, 2, ...n)$ are the correlation parameters.

3.2. Uncertainty Propagation Solution of Output Mean

In this method, if the input random variables do not follow normal distributions, an isoprobabilistic transformation should first be applied to transform the original input variables into independent ones in standardized normal space, i.e., $\boldsymbol{U} = T(\boldsymbol{X})$, where $\boldsymbol{U} = [U_1, U_2, ..., U_{n_{\boldsymbol{X}}}]^{\mathrm{T}}$ is the vector of standard normal variables. Then, Eq. (6) can be rewritten as follows:

$$G = g(T^{-1}(\boldsymbol{U}), \boldsymbol{Y}, \boldsymbol{Z}) = \mathcal{G}(\boldsymbol{U}, \boldsymbol{Y}, \boldsymbol{Z}) \tag{17}$$

Two types of transformations can be used, the Rosenblatt and Nataf transformations [39, 40]. For convenience of expression, let $\boldsymbol{W} = \left[\boldsymbol{U}^{\mathrm{T}}, \boldsymbol{Y}^{\mathrm{T}}, \boldsymbol{Z}^{\mathrm{T}}\right]$ and $\boldsymbol{P} = \left[\boldsymbol{Y}^{\mathrm{T}}, \boldsymbol{Z}^{\mathrm{T}}\right]$. Because the output mean and the output variance are functions of $\boldsymbol{y}$ and $\boldsymbol{z}$, the Gaussian correlation function (as shown in Eq. (16)) of LF Kriging model can be rewritten as follows:

$$\begin{aligned}
\psi_{\mathrm{c}}\left(\boldsymbol{w}, \boldsymbol{w}^{'}\right) &= \exp\left\{-\sum_{k=1}^{n_{\boldsymbol{X}}} \theta_{\mathrm{c}}^{(k)}\left(u^{(k)}, u^{'(k)}\right)^{2} - \sum_{k=1}^{n_{\boldsymbol{Y}}+n_{\boldsymbol{Z}}} \theta_{\mathrm{c}}^{(n_{\boldsymbol{X}}+k)}\left(p^{(k)}, p^{'(k)}\right)^{2}\right\} \\
&= \exp\left\{-\sum_{k=1}^{n_{\boldsymbol{X}}} \theta_{\mathrm{c}}^{(k)}\left(u^{(k)}, u^{'(k)}\right)^{2}\right\} \exp\left\{-\sum_{k=1}^{n_{\boldsymbol{Y}}+n_{\boldsymbol{Z}}} \theta_{\mathrm{c}}^{(n_{\boldsymbol{X}}+k)}\left(p^{(k)}, p^{'(k)}\right)^{2}\right\} \\
&= \gamma_{\boldsymbol{u}\mathrm{c}}\left(\boldsymbol{u}, \boldsymbol{u}^{'}\right)\gamma_{\boldsymbol{p}\mathrm{c}}\left(\boldsymbol{p}, \boldsymbol{p}^{'}\right)
\end{aligned} \tag{18}$$

where $\boldsymbol{w}$ and $\boldsymbol{w}^{'}$ are two arbitrary realizations of $\boldsymbol{W}$, $\boldsymbol{u}$ and $\boldsymbol{u}^{'}$ are two arbitrary realizations of $\boldsymbol{U}$, $\boldsymbol{p}$ and $\boldsymbol{p}^{'}$ are two arbitrary realizations of $\boldsymbol{P}$. Similarly, the correlation function of the difference Kriging model can be expressed as follows:

$$\begin{aligned}
\psi_{\mathrm{d}}\left(\boldsymbol{w}, \boldsymbol{w}^{'}\right) &= \exp\left\{-\sum_{k=1}^{n_{\boldsymbol{X}}} \theta_{\mathrm{d}}^{(k)}\left(u^{(k)}, u^{'(k)}\right)^{2}\right\} \exp\left\{-\sum_{k=1}^{n_{\boldsymbol{Y}}+n_{\boldsymbol{Z}}} \theta_{\mathrm{d}}^{(n_{\boldsymbol{X}}+k)}\left(p^{(k)}, p^{'(k)}\right)^{2}\right\} \\
&= \gamma_{\boldsymbol{u}\mathrm{d}}\left(\boldsymbol{u}, \boldsymbol{u}^{'}\right)\gamma_{\boldsymbol{p}\mathrm{d}}\left(\boldsymbol{p}, \boldsymbol{p}^{'}\right)
\end{aligned} \tag{19}$$

In this setting, the matrices of LF and HF training samples are $\boldsymbol{D}_{\mathrm{c}} = (\boldsymbol{w}_{\mathrm{c}}^{(1)}, \boldsymbol{w}_{\mathrm{c}}^{(2)}, ..., \boldsymbol{w}_{\mathrm{c}}^{(n_{\mathrm{c}})})^{\mathrm{T}}$ and $\boldsymbol{D}_{\mathrm{e}} = (\boldsymbol{w}_{\mathrm{e}}^{(1)}, \boldsymbol{w}_{\mathrm{e}}^{(2)}, ..., \boldsymbol{w}_{\mathrm{e}}^{(n_{\mathrm{e}})})^{\mathrm{T}}$, respectively. Then, we employ the mean of Co-Kriging prediction $\hat{y}_{\mathrm{e}}(\boldsymbol{w})$ to replace the real response G to obtain the analytical expression of the output mean $u_g(\boldsymbol{y}, \boldsymbol{z})$. It should be noted that $u_g(\boldsymbol{y}, \boldsymbol{z})$ is also a random variable after the replacement, whose mean $m_{\hat{g}}(\boldsymbol{y}, \boldsymbol{z})$ can be estimated by substituting Eqs. (12), (18) and (19) into Eq. (7):

$$\begin{aligned}
m_{\hat{g}}(\boldsymbol{y}, \boldsymbol{z}) &= \int_{\Omega_{\boldsymbol{U}}} \left[\hat{\mu} + \boldsymbol{c}_{(\boldsymbol{w})}^{\mathrm{T}} \boldsymbol{C}^{-1}\left(\boldsymbol{y}^{*} - \boldsymbol{1}\hat{\mu}\right)\right] f_{\boldsymbol{U}}(\boldsymbol{u})\mathrm{d}\boldsymbol{u} \\
&= \hat{\mu} + \left\{\int_{\Omega_{\boldsymbol{U}}} \boldsymbol{c}_{(\boldsymbol{w})}^{\mathrm{T}} f_{\boldsymbol{U}}(\boldsymbol{u})\mathrm{d}\boldsymbol{u}\right\} \boldsymbol{F}_{\boldsymbol{c}}
\end{aligned} \tag{20}$$

where

$$\boldsymbol{F}_{\boldsymbol{c}} = \left[\boldsymbol{C}^{-1}\left(\boldsymbol{y}^{*} - \mathbf{1}\hat{\mu}\right)\right] \tag{21}$$

$$\boldsymbol{c}_{(\boldsymbol{w})} = \begin{bmatrix} \rho\sigma_{\mathrm{c}}^{2}\boldsymbol{\psi}_{\mathrm{c}}\left(\boldsymbol{D}_{\mathrm{c}}, \boldsymbol{w}\right) \\ \rho^{2}\sigma_{\mathrm{c}}^{2}\boldsymbol{\psi}_{\mathrm{c}}\left(\boldsymbol{D}_{\mathrm{e}}, \boldsymbol{w}\right) + \sigma_{\mathrm{d}}^{2}\boldsymbol{\psi}_{\mathrm{d}}\left(\boldsymbol{D}_{\mathrm{e}}, \boldsymbol{w}\right) \end{bmatrix}$$
$$= \begin{bmatrix} \rho\sigma_{\mathrm{c}}^{2}\gamma_{\boldsymbol{u}\mathrm{c}}(\boldsymbol{u}_{\mathrm{c}}^{(1)}, \boldsymbol{u})\gamma_{\boldsymbol{p}\mathrm{c}}(\boldsymbol{p}_{\mathrm{c}}^{(1)}, \boldsymbol{p}) \\ \rho\sigma_{\mathrm{c}}^{2}\gamma_{\boldsymbol{u}\mathrm{c}}(\boldsymbol{u}_{\mathrm{c}}^{(2)}, \boldsymbol{u})\gamma_{\boldsymbol{p}\mathrm{c}}(\boldsymbol{p}_{\mathrm{c}}^{(2)}, \boldsymbol{p}) \\ \vdots \\ \rho\sigma_{\mathrm{c}}^{2}\gamma_{\boldsymbol{u}\mathrm{c}}(\boldsymbol{u}_{\mathrm{c}}^{(n_{\mathrm{c}})}, \boldsymbol{u})\gamma_{\boldsymbol{p}\mathrm{c}}(\boldsymbol{p}_{\mathrm{c}}^{(n_{\mathrm{c}})}, \boldsymbol{p}) \\ \rho^{2}\sigma_{\mathrm{c}}^{2}\gamma_{\boldsymbol{u}\mathrm{c}}(\boldsymbol{u}_{\mathrm{e}}^{(1)}, \boldsymbol{u})\gamma_{\boldsymbol{p}\mathrm{c}}(\boldsymbol{p}_{\mathrm{e}}^{(1)}, \boldsymbol{p}) + \sigma_{\mathrm{d}}^{2}\gamma_{\boldsymbol{u}\mathrm{d}}(\boldsymbol{u}_{\mathrm{e}}^{(1)}, \boldsymbol{u})\gamma_{\boldsymbol{p}\mathrm{d}}(\boldsymbol{p}_{\mathrm{e}}^{(1)}, \boldsymbol{p}) \\ \vdots \\ \rho^{2}\sigma_{\mathrm{c}}^{2}\gamma_{\boldsymbol{u}\mathrm{c}}(\boldsymbol{u}_{\mathrm{e}}^{(n_{\mathrm{e}})}, \boldsymbol{u})\gamma_{\boldsymbol{p}\mathrm{c}}(\boldsymbol{p}_{\mathrm{e}}^{(n_{\mathrm{e}})}, \boldsymbol{p}) + \sigma_{\mathrm{d}}^{2}\gamma_{\boldsymbol{u}\mathrm{d}}(\boldsymbol{u}_{\mathrm{e}}^{(n_{\mathrm{e}})}, \boldsymbol{u})\gamma_{\boldsymbol{p}\mathrm{d}}(\boldsymbol{p}_{\mathrm{e}}^{(n_{\mathrm{e}})}, \boldsymbol{p}) \end{bmatrix} \tag{22}$$

$\Omega_{\boldsymbol{U}}$ denotes the value domain of $\boldsymbol{U}$, and $f_{\boldsymbol{U}}(\boldsymbol{u})$ is the joint PDF of $\boldsymbol{U}$ with the corresponding mean vector and covariance matrix being $\boldsymbol{b}$ and $\boldsymbol{B}$, respectively.

To calculate the integral in Eq. (20), rewrite the vector $\boldsymbol{c}_{(\boldsymbol{w})}$ into two parts, where $\boldsymbol{\gamma}_{\mathrm{c}}^{(i)}\,(i = 1, 2, ..., n_{\mathrm{c}})$ are the first n_{c} elements in $\boldsymbol{c}_{(\boldsymbol{w})}$, and $\boldsymbol{\gamma}_{\mathrm{e}}^{(j)}\,(j = 1, 2, ..., n_{\mathrm{e}})$ are the last n_{e} elements in $\boldsymbol{c}_{(\boldsymbol{w})}$. Then, $\boldsymbol{\gamma}_{\mathrm{c}}^{(i)} f_{\boldsymbol{U}}(\boldsymbol{u})\,(i = 1, 2, ..., n_{\mathrm{c}})$ can be expressed as follows:

$$\boldsymbol{\gamma}_{\mathrm{c}}^{(i)} f_{\boldsymbol{U}}(\boldsymbol{u}) = \rho\sigma_{\mathrm{c}}^{2}\left(2\pi\right)^{\frac{n}{2}}\left|\boldsymbol{A}_{\mathrm{c}}\right|^{\frac{1}{2}} f_{\mathrm{cc}}^{(i)}\left(\boldsymbol{u}\right) f_{\boldsymbol{U}}\left(\boldsymbol{u}\right)\gamma_{\boldsymbol{p}\mathrm{c}}\left(\boldsymbol{p}_{\mathrm{c}}^{(i)}, \boldsymbol{p}\right) \tag{23}$$

where

$$f_{\mathrm{cc}}^{(i)}\left(\boldsymbol{u}\right) = \left(2\pi\right)^{-\frac{n}{2}}\left|\boldsymbol{A}_{\mathrm{c}}\right|^{-\frac{1}{2}}\exp\left\{-\frac{1}{2}\left(\boldsymbol{u}_{\mathrm{c}}^{(i)} - \boldsymbol{u}\right)^{\mathrm{T}}\boldsymbol{A}_{\mathrm{c}}^{-1}\left(\boldsymbol{u}_{\mathrm{c}}^{(i)} - \boldsymbol{u}\right)\right\} \tag{24}$$

and $\boldsymbol{A}_{\mathrm{c}} = \mathrm{diag}\left(\frac{1}{2\theta_{\mathrm{c}}^{(1)}}, \frac{1}{2\theta_{\mathrm{c}}^{(2)}}, ..., \frac{1}{2\theta_{\mathrm{c}}^{(n_{\boldsymbol{X}})}}\right)$. Similarly, $\boldsymbol{\gamma}_{\mathrm{e}}^{(j)} f_{\boldsymbol{U}}(\boldsymbol{u})\,(j = 1, 2, ..., n_{\mathrm{e}})$ can be expressed as follows:

$$\boldsymbol{\gamma}_{\mathrm{e}}^{(j)} f_{\boldsymbol{U}}(\boldsymbol{u}) = \left(2\pi\right)^{\frac{n}{2}}\left(\rho^{2}\sigma_{\mathrm{c}}^{2}\left|\boldsymbol{A}_{\mathrm{c}}\right|^{\frac{1}{2}} f_{\mathrm{ce}}^{(j)}\left(\boldsymbol{u}\right)\gamma_{\boldsymbol{p}\mathrm{c}}\left(\boldsymbol{p}_{\mathrm{e}}^{(j)}, \boldsymbol{p}\right) + \sigma_{\mathrm{d}}^{2}\left|\boldsymbol{A}_{\mathrm{d}}\right|^{\frac{1}{2}} f_{\mathrm{de}}^{(j)}\left(\boldsymbol{u}\right)\gamma_{\boldsymbol{p}\mathrm{d}}\left(\boldsymbol{p}_{\mathrm{e}}^{(j)}, \boldsymbol{p}\right)\right) f_{\boldsymbol{U}}\left(\boldsymbol{u}\right) \tag{25}$$

where

$$f_{\mathrm{ce}}^{(j)}(\boldsymbol{u}) = (2\pi)^{-\frac{n}{2}} |\boldsymbol{A}_{\mathrm{c}}|^{-\frac{1}{2}} \exp\left\{-\frac{1}{2}\left(\boldsymbol{u}_{\mathrm{e}}^{(j)} - \boldsymbol{u}\right)^{\mathrm{T}} \boldsymbol{A}_{\mathrm{c}}^{-1} \left(\boldsymbol{u}_{\mathrm{e}}^{(j)} - \boldsymbol{u}\right)\right\} \tag{26}$$

$$f_{\mathrm{de}}^{(j)}(\boldsymbol{u}) = (2\pi)^{-\frac{n}{2}} |\boldsymbol{A}_{\mathrm{d}}|^{-\frac{n}{2}} \exp\left\{-\frac{1}{2}\left(\boldsymbol{u}_{\mathrm{e}}^{(j)} - \boldsymbol{u}\right)^{\mathrm{T}} \boldsymbol{A}_{\mathrm{d}}^{-1} \left(\boldsymbol{u}_{\mathrm{e}}^{(j)} - \boldsymbol{u}\right)\right\} \tag{27}$$

and $\boldsymbol{A}_{\mathrm{d}} = \mathrm{diag}\left(\frac{1}{2\theta_{\mathrm{d}}^{(1)}}, \frac{1}{2\theta_{\mathrm{d}}^{(2)}}, ..., \frac{1}{2\theta_{\mathrm{d}}^{(n_{\boldsymbol{X}})}}\right)$, respectively. $f_{\mathrm{cc}}^{(i)}(\boldsymbol{u})$, $f_{\mathrm{ce}}^{(j)}(\boldsymbol{u})$, $f_{\mathrm{de}}^{(j)}(\boldsymbol{u})$ and $f_{\boldsymbol{U}}(\boldsymbol{u})$ are four joint Gaussian PDFs about the $n_{\boldsymbol{X}}$-dimension random variable $\boldsymbol{U}$, and the product of two Gaussian PDFs generates another un-normalized Gaussian PDF [41]. Accordingly, the three products, i.e., $f_{\mathrm{cc}}^{(i)}(\boldsymbol{u}) f_{\boldsymbol{U}}(\boldsymbol{u})$, $f_{\mathrm{ce}}^{(j)}(\boldsymbol{u}) f_{\boldsymbol{U}}(\boldsymbol{u})$, and $f_{\mathrm{de}}^{(j)}(\boldsymbol{u}) f_{\boldsymbol{U}}(\boldsymbol{u})$ can be derived as follows [41]:

$$f_{\mathrm{cc}}^{(i)}(\boldsymbol{u}) f_{\boldsymbol{U}}(\boldsymbol{u}) = (2\pi)^{-\frac{n}{2}} |\boldsymbol{A}_{\mathrm{c}} + \boldsymbol{B}|^{-\frac{1}{2}} \exp\left\{-\frac{1}{2}\left(\boldsymbol{u}_{\mathrm{c}}^{(i)} - \boldsymbol{b}\right)^{\mathrm{T}} (\boldsymbol{A}_{\mathrm{c}} + \boldsymbol{B})^{-1} \left(\boldsymbol{u}_{\mathrm{c}}^{(i)} - \boldsymbol{b}\right)\right\} f'_{\boldsymbol{U}}(\boldsymbol{u}) \tag{28}$$

$$f_{\mathrm{ce}}^{(j)}(\boldsymbol{u}) f_{\boldsymbol{U}}(\boldsymbol{u}) = (2\pi)^{-\frac{n}{2}} |\boldsymbol{A}_{\mathrm{c}} + \boldsymbol{B}|^{-\frac{1}{2}} \exp\left\{-\frac{1}{2}\left(\boldsymbol{u}_{\mathrm{e}}^{(j)} - \boldsymbol{b}\right)^{\mathrm{T}} (\boldsymbol{A}_{\mathrm{c}} + \boldsymbol{B})^{-1} \left(\boldsymbol{u}_{\mathrm{e}}^{(j)} - \boldsymbol{b}\right)\right\} f''_{\boldsymbol{U}}(\boldsymbol{u}) \tag{29}$$

$$f_{\mathrm{de}}^{(j)}(\boldsymbol{u}) f_{\boldsymbol{U}}(\boldsymbol{u}) = (2\pi)^{-\frac{n}{2}} |\boldsymbol{A}_{\mathrm{d}} + \boldsymbol{B}|^{-\frac{1}{2}} \exp\left\{-\frac{1}{2}\left(\boldsymbol{u}_{\mathrm{e}}^{(j)} - \boldsymbol{b}\right)^{\mathrm{T}} (\boldsymbol{A}_{\mathrm{d}} + \boldsymbol{B})^{-1} \left(\boldsymbol{u}_{\mathrm{e}}^{(j)} - \boldsymbol{b}\right)\right\} f'''_{\boldsymbol{U}}(\boldsymbol{u}) \tag{30}$$

where $f'_{\boldsymbol{U}}(\boldsymbol{u})$, $f''_{\boldsymbol{U}}(\boldsymbol{u})$ and $f'''_{\boldsymbol{U}}(\boldsymbol{u})$ are also joint Gaussian PDFs with the mean vectors $\bar{\boldsymbol{u}}'$, $\bar{\boldsymbol{u}}''$, $\bar{\boldsymbol{u}}'''$ and covariance matrices $\boldsymbol{Q}'$, $\boldsymbol{Q}''$, $\boldsymbol{Q}'''$, in which $\boldsymbol{Q}' = \boldsymbol{Q}'' = \left(\boldsymbol{A}_{\mathrm{c}}^{-1} + \boldsymbol{B}^{-1}\right)^{-1}$, $\boldsymbol{Q}''' = \left(\boldsymbol{A}_{\mathrm{d}}^{-1} + \boldsymbol{B}^{-1}\right)^{-1}$, $\bar{\boldsymbol{u}}' = \boldsymbol{Q}'\left(\boldsymbol{A}_{\mathrm{c}}^{-1}\boldsymbol{u}_{\mathrm{c}}^{(i)} + \boldsymbol{B}^{-1}\boldsymbol{b}\right)$, $\bar{\boldsymbol{u}}'' = \boldsymbol{Q}''\left(\boldsymbol{A}_{\mathrm{c}}^{-1}\boldsymbol{u}_{\mathrm{e}}^{(j)} + \boldsymbol{B}^{-1}\boldsymbol{b}\right)$, and $\bar{\boldsymbol{u}}''' = \boldsymbol{Q}'''\left(\boldsymbol{A}_{\mathrm{d}}^{-1}\boldsymbol{u}_{\mathrm{e}}^{(j)} + \boldsymbol{B}^{-1}\boldsymbol{b}\right)$, respectively.

Substituting Eq. (28) into Eq. (23), Eq. (29) and (30) into Eq. (25), the integral in Eq. (20) can be obtained by:

$$\begin{aligned}
\int_{\Omega_{\boldsymbol{U}}} \boldsymbol{c}_{(\boldsymbol{w})}^{\mathrm{T}} f_{\boldsymbol{U}}(\boldsymbol{u}) \mathrm{d}\boldsymbol{u} &= \left[\beta_{\mathrm{c}}^{(1)}, \beta_{\mathrm{c}}^{(2)}, ..., \beta_{\mathrm{c}}^{(n_{\mathrm{c}})}, \beta_{\mathrm{e}}^{(1)}, \beta_{\mathrm{e}}^{(2)}, ..., \beta_{\mathrm{e}}^{(n_{\mathrm{e}})}\right] \\
&= \left[\boldsymbol{\beta}_{\mathrm{c}}^{(i)}, \boldsymbol{\beta}_{\mathrm{e}}^{(j)}\right] \quad (i = 1, 2, ..., n_{\mathrm{c}}; j = 1, 2, ..., n_{\mathrm{e}}) \\
&= \boldsymbol{\beta}
\end{aligned} \tag{31}$$

where

$$\boldsymbol{\beta}_{\mathrm{c}}^{(i)} = \rho\sigma_{\mathrm{c}}^2 |\boldsymbol{A}_{\mathrm{c}}|^{\frac{1}{2}} |\boldsymbol{A}_{\mathrm{c}} + \boldsymbol{B}|^{-\frac{1}{2}} \exp\left\{-\frac{1}{2}\left(\boldsymbol{u}_{\mathrm{c}}^{(i)} - \boldsymbol{b}\right)^{\mathrm{T}} (\boldsymbol{A}_{\mathrm{c}} + \boldsymbol{B})^{-1} \left(\boldsymbol{u}_{\mathrm{c}}^{(i)} - \boldsymbol{b}\right)\right\} \gamma_{\boldsymbol{p}\mathrm{c}}\left(\boldsymbol{p}_{\mathrm{c}}^{(i)}, \boldsymbol{p}\right) \tag{32}$$

$$
\begin{aligned}
\boldsymbol{\beta}_{\mathrm{e}}^{(j)}=&\rho^{2}\sigma_{\mathrm{c}}^{2}\left|\boldsymbol{A}_{\mathrm{c}}\right|^{\frac{1}{2}}\left|\boldsymbol{A}_{\mathrm{c}}+\boldsymbol{B}\right|^{-\frac{1}{2}}\exp\left\{-\frac{1}{2}\left(\boldsymbol{u}_{\mathrm{e}}^{(j)}-\boldsymbol{b}\right)^{\mathrm{T}}\left(\boldsymbol{A}_{\mathrm{c}}+\boldsymbol{B}\right)^{-1}\left(\boldsymbol{u}_{\mathrm{e}}^{(j)}-\boldsymbol{b}\right)\right\}\gamma_{\boldsymbol{p}\mathrm{c}}\left(\boldsymbol{p}_{\mathrm{e}}^{(j)},\boldsymbol{p}\right)\\
&+\sigma_{\mathrm{d}}^{2}\left|\boldsymbol{A}_{\mathrm{d}}\right|^{\frac{1}{2}}\left|\boldsymbol{A}_{\mathrm{d}}+\boldsymbol{B}\right|^{-\frac{1}{2}}\exp\left\{-\frac{1}{2}\left(\boldsymbol{u}_{\mathrm{e}}^{(j)}-\boldsymbol{b}\right)^{\mathrm{T}}\left(\boldsymbol{A}_{\mathrm{d}}+\boldsymbol{B}\right)^{-1}\left(\boldsymbol{u}_{\mathrm{e}}^{(j)}-\boldsymbol{b}\right)\right\}\gamma_{\boldsymbol{p}\mathrm{d}}\left(\boldsymbol{p}_{\mathrm{e}}^{(j)},\boldsymbol{p}\right)
\end{aligned}
\tag{33}
$$

Substituting Eq. (31) into Eq. (20), the analytical solution of $m_{\hat{g}}(\boldsymbol{y},\boldsymbol{z})$ can be estimated as follows:

$$
m_{\hat{g}}(\boldsymbol{y},\boldsymbol{z})=\hat{\mu}+\boldsymbol{\beta}\boldsymbol{F}_{\boldsymbol{c}}
\tag{34}
$$

It should be pointed out that all parameters in Eq. (34) are available based on the constructed Co-Kriging model. Given a value of $\boldsymbol{p}$ (i.e., $(\boldsymbol{y},\boldsymbol{z})$), the mean of the performance function can be estimated analytically.

In the above derivation, the mean of $u_g(\boldsymbol{y},\boldsymbol{z})$ is derived by replacing the real response G with the mean of the Co-Kriging prediction $\hat{y}_{\mathrm{e}}\left(\boldsymbol{w}\right)$, where epistemic uncertainty is introduced. In the following text, we will also derive the analytical solution of the variance of $u_g(\boldsymbol{y},\boldsymbol{z})$, which is adopted to measure the epistemic uncertainty in $u_g(\boldsymbol{y},\boldsymbol{z})$.

The variance of $u_g(\boldsymbol{y},\boldsymbol{z})$ is defined as follows:

$$
\begin{aligned}
s_{\hat{g}}^{2}\left(\boldsymbol{y},\boldsymbol{z}\right)&=\int_{\Omega_{\hat{g}}}\left[\int_{\Omega_{\boldsymbol{U}}}\hat{g}\left(\boldsymbol{u},\boldsymbol{y},\boldsymbol{z}\right)f_{\boldsymbol{U}}\left(\boldsymbol{u}\right)\mathrm{d}\boldsymbol{u}-m_{\hat{g}}\left(\boldsymbol{y},\boldsymbol{z}\right)\right]^{2}f\left(\hat{g}\right)\mathrm{d}\hat{g}\\
&=\int_{\Omega_{\hat{g}}}\left[\int_{\Omega_{\boldsymbol{U}}}\left[\hat{g}\left(\boldsymbol{u},\boldsymbol{y},\boldsymbol{z}\right)-m_{\hat{g}}\left(\boldsymbol{y},\boldsymbol{z}\right)\right]f_{\boldsymbol{U}}\left(\boldsymbol{u}\right)\mathrm{d}\boldsymbol{u}\right.\\
&\qquad\left.\int_{\Omega_{\boldsymbol{U}'}}\left[\hat{g}\left(\boldsymbol{u}',\boldsymbol{y},\boldsymbol{z}\right)-m_{\hat{g}}\left(\boldsymbol{y},\boldsymbol{z}\right)\right]f_{\boldsymbol{U}'}\left(\boldsymbol{u}'\right)\mathrm{d}\boldsymbol{u}'\right]f\left(\hat{g}\right)\mathrm{d}\hat{g}\\
&=\int_{\Omega_{\boldsymbol{U}}}\int_{\Omega_{\boldsymbol{U}'}}\mathrm{cov}\left(\left(\boldsymbol{u},\boldsymbol{y},\boldsymbol{z}\right),\left(\boldsymbol{u}',\boldsymbol{y},\boldsymbol{z}\right)\right)f_{\boldsymbol{U}}\left(\boldsymbol{u}\right)f_{\boldsymbol{U}'}\left(\boldsymbol{u}'\right)\mathrm{d}\boldsymbol{u}\mathrm{d}\boldsymbol{u}'
\end{aligned}
\tag{35}
$$

where $\hat{g}\left(\boldsymbol{u},\boldsymbol{y},\boldsymbol{z}\right)$ is the Co-Kriging model approximation of G, $\Omega_{\hat{g}}$ and $f\left(\hat{g}\right)$ denote the value domain and the PDF of $\hat{g}$. Based on Eq. (15), the prediction covariance $\mathrm{cov}\left(\boldsymbol{w},\boldsymbol{w}'\right)$ is expressed below:

$$
\mathrm{cov}\left(\boldsymbol{w},\boldsymbol{w}'\right)=\rho^{2}\sigma_{\mathrm{c}}^{2}\psi_{\mathrm{c}}\left(\boldsymbol{w},\boldsymbol{w}'\right)+\sigma_{\mathrm{d}}^{2}\psi_{\mathrm{d}}\left(\boldsymbol{w},\boldsymbol{w}'\right)-\boldsymbol{c}_{(\boldsymbol{w})}^{\mathrm{T}}\boldsymbol{C}^{-1}\boldsymbol{c}_{(\boldsymbol{w}')}
\tag{36}
$$

Substituting Eqs. (18), (19), (31) and (36) into Eq. (35), $s_{\hat{g}}^2(\boldsymbol{y},\boldsymbol{z})$ can be rewritten as follows:

$$\begin{aligned} s_{\hat{g}}^2(\boldsymbol{y},\boldsymbol{z}) =& \rho^2\sigma_{\mathrm{c}}^2 \int_{\Omega_{\boldsymbol{U}}}\int_{\Omega_{\boldsymbol{U}'}} \gamma_{\boldsymbol{u}\mathrm{c}}(\boldsymbol{u},\boldsymbol{u}') f_{\boldsymbol{U}}(\boldsymbol{u}) f_{\boldsymbol{U}'}(\boldsymbol{u}')\,\mathrm{d}\boldsymbol{u}\mathrm{d}\boldsymbol{u}' \\ &+ \sigma_{\mathrm{d}}^2 \int_{\Omega_{\boldsymbol{U}}}\int_{\Omega_{\boldsymbol{U}'}} \gamma_{\boldsymbol{u}\mathrm{d}}(\boldsymbol{u},\boldsymbol{u}') f_{\boldsymbol{U}}(\boldsymbol{u}) f_{\boldsymbol{U}'}(\boldsymbol{u}')\,\mathrm{d}\boldsymbol{u}\mathrm{d}\boldsymbol{u}' - \boldsymbol{\beta}\boldsymbol{C}^{-1}\boldsymbol{\beta}^{\mathrm{T}} \end{aligned} \tag{37}$$

in which $\int_{\Omega_{\boldsymbol{U}}}\int_{\Omega_{\boldsymbol{U}'}} \gamma_{\boldsymbol{u}\mathrm{c}}(\boldsymbol{u},\boldsymbol{u}') f_{\boldsymbol{U}}(\boldsymbol{u}) f_{\boldsymbol{U}'}(\boldsymbol{u}')\,\mathrm{d}\boldsymbol{u}\mathrm{d}\boldsymbol{u}'$ and $\int_{\Omega_{\boldsymbol{U}}}\int_{\Omega_{\boldsymbol{U}'}} \gamma_{\boldsymbol{u}\mathrm{d}}(\boldsymbol{u},\boldsymbol{u}') f_{\boldsymbol{U}}(\boldsymbol{u}) f_{\boldsymbol{U}'}(\boldsymbol{u}')\,\mathrm{d}\boldsymbol{u}\mathrm{d}\boldsymbol{u}'$ are given as [42, 43]:

$$\int_{\Omega_{\boldsymbol{U}}}\int_{\Omega_{\boldsymbol{U}'}} \gamma_{\boldsymbol{u}\mathrm{c}}(\boldsymbol{u},\boldsymbol{u}') f_{\boldsymbol{U}}(\boldsymbol{u}) f_{\boldsymbol{U}'}(\boldsymbol{u}')\,\mathrm{d}\boldsymbol{u}\mathrm{d}\boldsymbol{u}' = \left|2\boldsymbol{A}_{\mathrm{c}}{}^{-1}\boldsymbol{B}+\boldsymbol{I}\right|^{-\frac{1}{2}} \tag{38}$$

$$\int_{\Omega_{\boldsymbol{U}}}\int_{\Omega_{\boldsymbol{U}'}} \gamma_{\boldsymbol{u}\mathrm{d}}(\boldsymbol{u},\boldsymbol{u}') f_{\boldsymbol{U}}(\boldsymbol{u}) f_{\boldsymbol{U}'}(\boldsymbol{u}')\,\mathrm{d}\boldsymbol{u}\mathrm{d}\boldsymbol{u}' = \left|2\boldsymbol{A}_{\mathrm{d}}{}^{-1}\boldsymbol{B}+\boldsymbol{I}\right|^{-\frac{1}{2}} \tag{39}$$

Finally, the analytical solution of $s_{\hat{g}}^2(\boldsymbol{y},\boldsymbol{z})$ is obtained as follows:

$$s_{\hat{g}}^2(\boldsymbol{y},\boldsymbol{z}) = \rho^2\sigma_{\mathrm{c}}^2\left|2\boldsymbol{A}_{\mathrm{c}}{}^{-1}\boldsymbol{B}+\boldsymbol{I}\right|^{-\frac{1}{2}} + \sigma_{\mathrm{d}}^2\left|2\boldsymbol{A}_{\mathrm{d}}{}^{-1}\boldsymbol{B}+\boldsymbol{I}\right|^{-\frac{1}{2}} - \boldsymbol{\beta}\boldsymbol{C}^{-1}\boldsymbol{\beta}^{\mathrm{T}} \tag{40}$$

3.3. Uncertainty Propagation Solution of Output Variance

In order to obtain the analytical solution of the output variance $\sigma_g^2(\boldsymbol{y},\boldsymbol{z})$ defined in Eq. (8), we still resort to the mean of Co-Kriging prediction, and Eq. (8) can be rewritten as follows:

$$\begin{aligned} \sigma_g^2(\boldsymbol{y},\boldsymbol{z}) &= \int_{\Omega_{\boldsymbol{U}}} [g(\boldsymbol{u},\boldsymbol{y},\boldsymbol{z}) - u_g(\boldsymbol{y},\boldsymbol{z})]^2 f_{\boldsymbol{U}}(\boldsymbol{u})\mathrm{d}\boldsymbol{u} \\ &= \int_{\Omega_{\boldsymbol{U}}} \left[g^2(\boldsymbol{u},\boldsymbol{y},\boldsymbol{z}) + u_g^2(\boldsymbol{y},\boldsymbol{z}) - 2g(\boldsymbol{u},\boldsymbol{y},\boldsymbol{z})u_g(\boldsymbol{y},\boldsymbol{z})\right] f_{\boldsymbol{U}}(\boldsymbol{u})\mathrm{d}\boldsymbol{u} \\ &= \int_{\Omega_{\boldsymbol{U}}} \left[g^2(\boldsymbol{u},\boldsymbol{y},\boldsymbol{z}) - u_g^2(\boldsymbol{y},\boldsymbol{z})\right] f_{\boldsymbol{U}}(\boldsymbol{u})\mathrm{d}\boldsymbol{u} \\ &= \int_{\Omega_{\boldsymbol{U}}} \left[\hat{y}_{\mathrm{e}}^2(\boldsymbol{u},\boldsymbol{y},\boldsymbol{z}) - u_g^2(\boldsymbol{y},\boldsymbol{z})\right] f_{\boldsymbol{U}}(\boldsymbol{u})\mathrm{d}\boldsymbol{u} \\ &= \hat{\mu}^2 + 2\hat{\mu}\boldsymbol{\beta}\boldsymbol{C}^{-1}\boldsymbol{\beta}^{\mathrm{T}}\boldsymbol{F}_{\boldsymbol{c}} - u_g^2(\boldsymbol{y},\boldsymbol{z}) + \boldsymbol{F}_{\boldsymbol{c}}^{\mathrm{T}}\left[\int_{\Omega_{\boldsymbol{U}}} \boldsymbol{c}_{(\boldsymbol{w})}\boldsymbol{c}_{(\boldsymbol{w})}^{\mathrm{T}} f_{\boldsymbol{U}}(\boldsymbol{u})\mathrm{d}\boldsymbol{u}\right]\boldsymbol{F}_{\boldsymbol{c}} \end{aligned} \tag{41}$$

where $u_g^2(\boldsymbol{y},\boldsymbol{z})$ can be estimated by Eq. (34), $\boldsymbol{c}_{(\boldsymbol{w})}\boldsymbol{c}_{(\boldsymbol{w})}^{\mathrm{T}}$ is a block matrix expressed as follows:

$$\boldsymbol{c}_{(\boldsymbol{w})}\boldsymbol{c}_{(\boldsymbol{w})}^{\mathrm{T}} = \begin{bmatrix} \boldsymbol{\gamma}_{\mathrm{cc}} & \boldsymbol{\gamma}_{\mathrm{ce}} \\ \boldsymbol{\gamma}_{\mathrm{ec}} & \boldsymbol{\gamma}_{\mathrm{ee}} \end{bmatrix} \tag{42}$$

in which $\boldsymbol{\gamma}_{\rm cc}$ is an $n_{\rm c}$-by-$n_{\rm c}$ matrix with the (i,j)-th entry $[\boldsymbol{\gamma}_{\rm cc}]_{ij}=\gamma_{\rm c}^{(i)}\gamma_{\rm c}^{(j)}$, $\boldsymbol{\gamma}_{\rm ce}$ is an $n_{\rm c}$-by-$n_{\rm e}$ matrix with the (i,j)-th entry $[\boldsymbol{\gamma}_{\rm ce}]_{ij}=\gamma_{\rm c}^{(i)}\gamma_{\rm e}^{(j)}$, $\boldsymbol{\gamma}_{\rm ec}$ is the transpose matrix of $\boldsymbol{\gamma}_{\rm ce}$, and $\boldsymbol{\gamma}_{\rm ee}$ is an $n_{\rm e}$-by-$n_{\rm e}$ matrix with the (i,j)-th entry $[\boldsymbol{\gamma}_{\rm ee}]_{ij}=\gamma_{\rm e}^{(i)}\gamma_{\rm e}^{(j)}$.

Take the (i,j)-th entry of matrix $\boldsymbol{\gamma}_{\rm cc}$ as an example, the resulting integral is calculated as follows:

$$\begin{aligned}\int_{\Omega_{\boldsymbol{U}}}\gamma_{\rm c}^{(i)}\gamma_{\rm c}^{(j)}f_{\boldsymbol{U}}\left(\boldsymbol{u}\right)\mathrm{d}\boldsymbol{u}&=\left(\rho\sigma_{\rm c}^2\left(2\pi\right)^{\frac{n}{2}}\left|\boldsymbol{A}_{\rm c}\right|^{\frac{1}{2}}\right)^2\left[\int_{\Omega_{\boldsymbol{U}}}f_{\rm cc}^{(i)}(\boldsymbol{u})f_{\rm cc}^{(j)}(\boldsymbol{u})f_{\boldsymbol{U}}\left(\boldsymbol{u}\right)\mathrm{d}\boldsymbol{u}\right]\gamma_{\boldsymbol{p}\rm c}\left(\boldsymbol{p}_{\rm c}^{(i)},\boldsymbol{p}\right)\gamma_{\boldsymbol{p}\rm c}\left(\boldsymbol{p}_{\rm c}^{(j)},\boldsymbol{p}\right)\\&=\rho^2\sigma_{\rm c}^4\left|\boldsymbol{A}_{\rm c}\right|H_1\left(\boldsymbol{u}_{\rm c}^{(i)}\right)H_2\left(\boldsymbol{u}_{\rm c}^{(j)}\right)\gamma_{\boldsymbol{p}\rm c}\left(\boldsymbol{p}_{\rm c}^{(i)},\boldsymbol{p}\right)\gamma_{\boldsymbol{p}\rm c}\left(\boldsymbol{p}_{\rm c}^{(j)},\boldsymbol{p}\right)\end{aligned}\tag{43}$$

where

$$H_1\left(\boldsymbol{u}_{\rm c}^{(i)}\right)=\left|\boldsymbol{A}_{\rm c}+\boldsymbol{B}\right|^{-\frac{1}{2}}\exp\left\{-\frac{1}{2}\left(\boldsymbol{u}_{\rm c}^{(i)}-\boldsymbol{b}\right)^{\rm T}\left(\boldsymbol{A}_{\rm c}+\boldsymbol{B}\right)^{-1}\left(\boldsymbol{u}_{\rm c}^{(i)}-\boldsymbol{b}\right)\right\}\tag{44}$$

$$H_2\left(\boldsymbol{u}_{\rm c}^{(j)}\right)=\left|\boldsymbol{Q}'+\boldsymbol{A}_{\rm c}\right|^{-\frac{1}{2}}\exp\left\{-\frac{1}{2}\left(\bar{\boldsymbol{u}}'-\boldsymbol{u}_{\rm c}^{(j)}\right)^{\rm T}\left(\boldsymbol{Q}'+\boldsymbol{A}_{\rm c}\right)^{-1}\left(\bar{\boldsymbol{u}}'-\boldsymbol{u}_{\rm c}^{(j)}\right)\right\}\tag{45}$$

Similarly, the integral of the (i,j)-th entry of matrix $\boldsymbol{\gamma}_{\rm ce}$ can be obtained as follows:

$$\begin{aligned}&\int_{\Omega_{\boldsymbol{U}}}\gamma_{\rm c}^{(i)}\gamma_{\rm e}^{(j)}f_{\boldsymbol{U}}\left(\boldsymbol{u}\right)\mathrm{d}\boldsymbol{u}\\=&\rho^3\sigma_{\rm c}^4\left(2\pi\right)^n\left|\boldsymbol{A}_{\rm c}\right|\left[\int_{\Omega_{\boldsymbol{U}}}f_{\rm cc}^{(i)}\left(\boldsymbol{u}\right)f_{\rm ce}^{(j)}\left(\boldsymbol{u}\right)f_{\boldsymbol{U}}\left(\boldsymbol{u}\right)\mathrm{d}\boldsymbol{u}\right]\gamma_{\boldsymbol{p}\rm c}\left(\boldsymbol{p}_{\rm c}^{(i)},\boldsymbol{p}\right)\gamma_{\boldsymbol{p}\rm c}\left(\boldsymbol{p}_{\rm e}^{(j)},\boldsymbol{p}\right)\\&+\rho\sigma_{\rm c}^2\sigma_{\rm d}^2\left(2\pi\right)^n\left|\boldsymbol{A}_{\rm c}\right|^{\frac{1}{2}}\left|\boldsymbol{A}_{\rm d}\right|^{\frac{1}{2}}\left[\int_{\Omega_{\boldsymbol{U}}}f_{\rm cc}^{(i)}\left(\boldsymbol{u}\right)f_{\rm de}^{(j)}\left(\boldsymbol{u}\right)f_{\boldsymbol{U}}\left(\boldsymbol{u}\right)\mathrm{d}\boldsymbol{u}\right]\gamma_{\boldsymbol{p}\rm c}\left(\boldsymbol{p}_{\rm c}^{(i)},\boldsymbol{p}\right)\gamma_{\boldsymbol{p}\rm d}\left(\boldsymbol{p}_{\rm e}^{(j)},\boldsymbol{p}\right)\\=&\rho^3\sigma_{\rm c}^4\left|\boldsymbol{A}_{\rm c}\right|H_1\left(\boldsymbol{u}_{\rm c}^{(i)}\right)H_2\left(\boldsymbol{u}_{\rm e}^{(j)}\right)\gamma_{\boldsymbol{p}\rm c}\left(\boldsymbol{p}_{\rm c}^{(i)},\boldsymbol{p}\right)\gamma_{\boldsymbol{p}\rm c}\left(\boldsymbol{p}_{\rm e}^{(j)},\boldsymbol{p}\right)\\&+\rho\sigma_{\rm c}^2\sigma_{\rm d}^2\left|\boldsymbol{A}_{\rm c}\right|^{\frac{1}{2}}\left|\boldsymbol{A}_{\rm d}\right|^{\frac{1}{2}}H_1\left(\boldsymbol{u}_{\rm c}^{(i)}\right)H_3\left(\boldsymbol{u}_{\rm e}^{(j)}\right)\gamma_{\boldsymbol{p}\rm c}\left(\boldsymbol{p}_{\rm c}^{(i)},\boldsymbol{p}\right)\gamma_{\boldsymbol{p}\rm d}\left(\boldsymbol{p}_{\rm e}^{(j)},\boldsymbol{p}\right)\end{aligned}\tag{46}$$

where

$$H_3\left(\boldsymbol{u}_{\rm e}^{(j)}\right)=\left|\boldsymbol{Q}'+\boldsymbol{A}_{\rm d}\right|^{-\frac{1}{2}}\exp\left\{-\frac{1}{2}\left(\bar{\boldsymbol{u}}'-\boldsymbol{u}_{\rm e}^{(j)}\right)^{\rm T}\left(\boldsymbol{Q}'+\boldsymbol{A}_{\rm d}\right)^{-1}\left(\bar{\boldsymbol{u}}'-\boldsymbol{u}_{\rm e}^{(j)}\right)\right\}\tag{47}$$

Once again, the integral of the (i, j)-th entry of matrix $\boldsymbol{\gamma}_{\mathrm{ee}}$ is given as follows:

$$\begin{aligned}
&\int_{\Omega_{\boldsymbol{U}}} \gamma_{\mathrm{e}}^{(i)} \gamma_{\mathrm{e}}^{(j)} f_{\boldsymbol{U}}(\boldsymbol{u})\, \mathrm{d}\boldsymbol{u} \\
&= \rho^4 \sigma_{\mathrm{c}}^4 (2\pi)^n |\boldsymbol{A}_{\mathrm{c}}| \left[\int_{\Omega_{\boldsymbol{U}}} f_{\mathrm{ce}}^{(i)}(\boldsymbol{u})\, f_{\mathrm{ce}}^{(j)}(\boldsymbol{u})\, f_{\boldsymbol{U}}(\boldsymbol{u})\, \mathrm{d}\boldsymbol{u} \right] \gamma_{\boldsymbol{p}\mathrm{c}}\left(\boldsymbol{p}_{\mathrm{e}}^{(i)}, \boldsymbol{p}\right) \gamma_{\boldsymbol{p}\mathrm{c}}\left(\boldsymbol{p}_{\mathrm{e}}^{(j)}, \boldsymbol{p}\right) \\
&\quad + \rho^2 \sigma_{\mathrm{c}}^2 \sigma_{\mathrm{d}}^2 (2\pi)^n |\boldsymbol{A}_{\mathrm{c}}|^{\frac{1}{2}} |\boldsymbol{A}_{\mathrm{d}}|^{\frac{1}{2}} \left[\int_{\Omega_{\boldsymbol{U}}} f_{\mathrm{ce}}^{(i)}(\boldsymbol{u})\, f_{\mathrm{de}}^{(j)}(\boldsymbol{u})\, f_{\boldsymbol{U}}(\boldsymbol{u})\, \mathrm{d}\boldsymbol{u} \right] \gamma_{\boldsymbol{p}\mathrm{c}}\left(\boldsymbol{p}_{\mathrm{e}}^{(i)}, \boldsymbol{p}\right) \gamma_{\boldsymbol{p}\mathrm{d}}\left(\boldsymbol{p}_{\mathrm{e}}^{(j)}, \boldsymbol{p}\right) \\
&\quad + \rho^2 \sigma_{\mathrm{c}}^2 \sigma_{\mathrm{d}}^2 (2\pi)^n |\boldsymbol{A}_{\mathrm{c}}|^{\frac{1}{2}} |\boldsymbol{A}_{\mathrm{d}}|^{\frac{1}{2}} \left[\int_{\Omega_{\boldsymbol{U}}} f_{\mathrm{ce}}^{(j)}(\boldsymbol{u})\, f_{\mathrm{de}}^{(i)}(\boldsymbol{u})\, f_{\boldsymbol{U}}(\boldsymbol{u})\, \mathrm{d}\boldsymbol{u} \right] \gamma_{\boldsymbol{p}\mathrm{c}}\left(\boldsymbol{p}_{\mathrm{e}}^{(j)}, \boldsymbol{p}\right) \gamma_{\boldsymbol{p}\mathrm{d}}\left(\boldsymbol{p}_{\mathrm{e}}^{(i)}, \boldsymbol{p}\right) \\
&\quad + \sigma_{\mathrm{d}}^4 (2\pi)^n |\boldsymbol{A}_{\mathrm{d}}| \left[\int_{\Omega_{\boldsymbol{U}}} f_{\mathrm{de}}^{(i)}(\boldsymbol{u})\, f_{\mathrm{de}}^{(j)}(\boldsymbol{u})\, f_{\boldsymbol{U}}(\boldsymbol{u})\, \mathrm{d}\boldsymbol{u} \right] \gamma_{\boldsymbol{p}\mathrm{d}}\left(\boldsymbol{p}_{\mathrm{e}}^{(i)}, \boldsymbol{p}\right) \gamma_{\boldsymbol{p}\mathrm{d}}\left(\boldsymbol{p}_{\mathrm{e}}^{(j)}, \boldsymbol{p}\right) \\
&= \rho^4 \sigma_{\mathrm{c}}^4 |\boldsymbol{A}_{\mathrm{c}}|\, H_1\left(\boldsymbol{u}_{\mathrm{e}}^{(i)}\right) H_4\left(\boldsymbol{u}_{\mathrm{e}}^{(j)}\right) \gamma_{\boldsymbol{p}\mathrm{c}}\left(\boldsymbol{p}_{\mathrm{e}}^{(i)}, \boldsymbol{p}\right) \gamma_{\boldsymbol{p}\mathrm{c}}\left(\boldsymbol{p}_{\mathrm{e}}^{(j)}, \boldsymbol{p}\right) \\
&\quad + \rho^2 \sigma_{\mathrm{c}}^2 \sigma_{\mathrm{d}}^2 |\boldsymbol{A}_{\mathrm{c}}|^{\frac{1}{2}} |\boldsymbol{A}_{\mathrm{d}}|^{\frac{1}{2}} H_1\left(\boldsymbol{u}_{\mathrm{e}}^{(i)}\right) H_5\left(\boldsymbol{u}_{\mathrm{e}}^{(j)}\right) \gamma_{\boldsymbol{p}\mathrm{c}}\left(\boldsymbol{p}_{\mathrm{e}}^{(i)}, \boldsymbol{p}\right) \gamma_{\boldsymbol{p}\mathrm{d}}\left(\boldsymbol{p}_{\mathrm{e}}^{(j)}, \boldsymbol{p}\right) \\
&\quad + \rho^2 \sigma_{\mathrm{c}}^2 \sigma_{\mathrm{d}}^2 |\boldsymbol{A}_{\mathrm{c}}|^{\frac{1}{2}} |\boldsymbol{A}_{\mathrm{d}}|^{\frac{1}{2}} H_1\left(\boldsymbol{u}_{\mathrm{e}}^{(j)}\right) H_5\left(\boldsymbol{u}_{\mathrm{e}}^{(i)}\right) \gamma_{\boldsymbol{p}\mathrm{c}}\left(\boldsymbol{p}_{\mathrm{e}}^{(j)}, \boldsymbol{p}\right) \gamma_{\boldsymbol{p}\mathrm{d}}\left(\boldsymbol{p}_{\mathrm{e}}^{(i)}, \boldsymbol{p}\right) \\
&\quad + \sigma_{\mathrm{d}}^4 |\boldsymbol{A}_{\mathrm{d}}|\, H_6\left(\boldsymbol{u}_{\mathrm{e}}^{(i)}\right) H_7\left(\boldsymbol{u}_{\mathrm{e}}^{(j)}\right) \gamma_{\boldsymbol{p}\mathrm{d}}\left(\boldsymbol{p}_{\mathrm{e}}^{(i)}, \boldsymbol{p}\right) \gamma_{\boldsymbol{p}\mathrm{d}}\left(\boldsymbol{p}_{\mathrm{e}}^{(j)}, \boldsymbol{p}\right)
\end{aligned} \tag{48}$$

where

$$H_4\left(\boldsymbol{u}_{\mathrm{e}}^{(j)}\right) = |\boldsymbol{Q}'' + \boldsymbol{A}_{\mathrm{c}}|^{-\frac{1}{2}} \exp\left\{ -\frac{1}{2} \left(\bar{\boldsymbol{u}}'' - \boldsymbol{u}_{\mathrm{e}}^{(j)}\right)^{\mathrm{T}} (\boldsymbol{Q}'' + \boldsymbol{A}_{\mathrm{c}})^{-1} \left(\bar{\boldsymbol{u}}'' - \boldsymbol{u}_{\mathrm{e}}^{(j)}\right) \right\} \tag{49}$$

$$H_5\left(\boldsymbol{u}_{\mathrm{e}}^{(j)}\right) = |\boldsymbol{Q}'' + \boldsymbol{A}_{\mathrm{d}}|^{-\frac{1}{2}} \exp\left\{ -\frac{1}{2} \left(\bar{\boldsymbol{u}}'' - \boldsymbol{u}_{\mathrm{e}}^{(j)}\right)^{\mathrm{T}} (\boldsymbol{Q}'' + \boldsymbol{A}_{\mathrm{d}})^{-1} \left(\bar{\boldsymbol{u}}'' - \boldsymbol{u}_{\mathrm{e}}^{(j)}\right) \right\} \tag{50}$$

$$H_6\left(\boldsymbol{u}_{\mathrm{e}}^{(i)}\right) = |\boldsymbol{A}_{\mathrm{d}} + \boldsymbol{B}|^{-\frac{1}{2}} \exp\left\{ -\frac{1}{2} \left(\boldsymbol{u}_{\mathrm{e}}^{(i)} - \boldsymbol{b}\right)^{\mathrm{T}} (\boldsymbol{A}_{\mathrm{d}} + \boldsymbol{B})^{-1} \left(\boldsymbol{u}_{\mathrm{e}}^{(i)} - \boldsymbol{b}\right) \right\} \tag{51}$$

$$H_7\left(\boldsymbol{u}_{\mathrm{e}}^{(j)}\right) = \left|\boldsymbol{Q}''' + \boldsymbol{A}_{\mathrm{d}}\right|^{-\frac{1}{2}} \exp\left\{ -\frac{1}{2} \left(\bar{\boldsymbol{u}}''' - \boldsymbol{u}_{\mathrm{e}}^{(j)}\right)^{\mathrm{T}} \left(\boldsymbol{Q}''' + \boldsymbol{A}_{\mathrm{d}}\right)^{-1} \left(\bar{\boldsymbol{u}}''' - \boldsymbol{u}_{\mathrm{e}}^{(j)}\right) \right\} \tag{52}$$

Substituting Eqs. (43), (46) and (48) into Eq. (41) gives the analytical solution of the output variance $\sigma_g^2(\boldsymbol{y}, \boldsymbol{z})$, which is an explicit function of $\boldsymbol{p}$ (i.e., $(\boldsymbol{y}, \boldsymbol{z})$).

3.4. Adaptive hybrid uncertainty propagation

Recall that the primary goal is to estimate the output mean $u_g(\boldsymbol{y}, \boldsymbol{z})$ and the output variance $\sigma_g^2(\boldsymbol{y}, \boldsymbol{z})$, where epistemic uncertainty is introduced by the Co-Kriging model prediction. Hence, the active learning strategy should focus on reducing the epistemic uncertainty in $u_g(\boldsymbol{y}, \boldsymbol{z})$ and $\sigma_g^2(\boldsymbol{y}, \boldsymbol{z})$.

Based on the augmented expected improvement (AEI) function [44], an adaptive framework is established, where two stopping criteria are proposed for the single loop active learning. The analytical solutions for the mean and variance of $u_g(\boldsymbol{y}, \boldsymbol{z})$ given in Eqs. (34) and (40) are employed to facilitate the identification of new points:

$$\mathrm{AEI}\left(\boldsymbol{p}\right) = \left(m_{\hat{g}}(\boldsymbol{p}^{**}) - m_{\hat{g}}(\boldsymbol{p})\right) \Phi \left(\frac{m_{\hat{g}}(\boldsymbol{p}^{**}) - m_{\hat{g}}(\boldsymbol{p})}{s_{\hat{g}}\left(\boldsymbol{p}\right)} \right) + s_{\hat{g}}\left(\boldsymbol{p}\right) \varphi \left(\frac{m_{\hat{g}}(\boldsymbol{p}^{**}) - m_{\hat{g}}(\boldsymbol{p})}{s_{\hat{g}}\left(\boldsymbol{p}\right)} \right) \tag{53}$$

where $\boldsymbol{p}^{**}$ is determined by:

$$\boldsymbol{p}^{**} = \arg\max\left[-m_{\hat{g}}(\boldsymbol{p}) - c s_{\hat{g}}\left(\boldsymbol{p}\right)\right] \tag{54}$$

with $c = 1$; $\Phi\left(\cdot\right)$ and $\varphi\left(\cdot\right)$ are the cumulative distribution function (CDF) and the PDF of the standard normal distribution, respectively.

The computational steps of active learning are elaborated as below:

Step 1: Generation of candidate sample set Ω for random variables. In this paper, the Sobol's quasi-random sequence [45] is employed to generate low-discrepancy candidate samples of size N_Ω in standard normal space.

Step 2: Construction of the Co-Kriging model based on training samples $\boldsymbol{D}_\mathrm{c}$ and $\boldsymbol{D}_\mathrm{e}$ for LF and HF models. To ensure the uniformity of the initial samples and to capture the global approximation behavior of Co-Kriging, Latin Hypercube Sampling (LHS) is performed to generate initial training samples, where the cut level α of the fuzzy variables is set to 0 for sampling. Then, the real responses $\boldsymbol{y}_\mathrm{c}$ and $\boldsymbol{y}_\mathrm{e}$ of the LF and HF models at training samples are obtained.

Step 3: Calculation of the upper and lower bounds for the output mean $u_g(\boldsymbol{y}, \boldsymbol{z})$ and the output variance $\sigma_g^2(\boldsymbol{y}, \boldsymbol{z})$ at each cut level. Based on Eqs. (34) and (41), the bounds of $u_g(\boldsymbol{y}, \boldsymbol{z})$ and $\sigma_g^2(\boldsymbol{y}, \boldsymbol{z})$ at each cut level α can be collected by discretizing interval and fuzzy variables.

Step 4: Stopping criterion. In this paper, two efficient convergence criteria are established to stop the iteration. The first stopping criterion is defined as the maximum coefficient of variation (Cov) of $u_g(\boldsymbol{y}, \boldsymbol{z})$ at the lower and upper bounds:

$$\left[Cov^{(1)}, Cov^{(2)}, ..., Cov^{(n)}\right]_{\max} \leq e_1 \tag{55}$$

where $Cov^{(i)}\,(i = 1, 2, ..., n)$ denote all the Cov of $u_g(\boldsymbol{y}, \boldsymbol{z})$ at the lower and upper bounds, and e_1 is the error threshold. The first criterion can measure the accuracy of the lower and upper bounds of the output mean. In addition, the second criterion considers the maximum value of the AEI function:

$$\max\left(\mathrm{AEI}\left(\boldsymbol{p}\right)\right) \leq m_{\hat{g}}(\boldsymbol{p}^{**}) \cdot e_2 \tag{56}$$

where e_2 is a user-specified value. The left term in the second stopping criterion indicates by how much the maximum improvement is expected to be greater than $m_{\hat{g}}(\boldsymbol{p}^{**})$ and reflects the level of epistemic uncertainty in the Co-Kriging model. If both of the stopping criteria are consecutively satisfied for 2 iterations, stop the Co-Kriging update and return the bounds of $u_g(\boldsymbol{y}, \boldsymbol{z})$ and $\sigma_g^2(\boldsymbol{y}, \boldsymbol{z})$. Otherwise, go to step 5.

Step 5: Identification of the update point. The values of the interval and fuzzy variables for the new point (denoted as $(\boldsymbol{y}^*, \boldsymbol{z}^*)$) are adaptively determined by maximizing the learning function AEI shown in Eq. (53). The values of the interval and fuzzy variables are then fixed, and determine the values of the random variables from Ω by maximizing the expected improvement (EI) function based on LF and HF predictions:

$$\mathrm{EI_c}\left(\boldsymbol{x}\right) = \left(y_{\mathrm{c}}^{\min} - y_{\mathrm{c}}(\boldsymbol{x}, \boldsymbol{y}^*, \boldsymbol{z}^*)\right) \Phi\left(\frac{y_{\mathrm{c}}^{\min} - y_{\mathrm{c}}(\boldsymbol{x}, \boldsymbol{y}^*, \boldsymbol{z}^*)}{s_{\mathrm{c}}\left(\boldsymbol{x}, \boldsymbol{y}^*, \boldsymbol{z}^*\right)}\right) + s_{\mathrm{c}}\left(\boldsymbol{x}, \boldsymbol{y}^*, \boldsymbol{z}^*\right) \varphi\left(\frac{y_{\mathrm{c}}^{\min} - y_{\mathrm{c}}(\boldsymbol{x}, \boldsymbol{y}^*, \boldsymbol{z}^*)}{s_{\mathrm{c}}\left(\boldsymbol{x}, \boldsymbol{y}^*, \boldsymbol{z}^*\right)}\right) \tag{57}$$

$$\mathrm{EI_e}\left(\boldsymbol{x}\right) = \left(y_{\mathrm{e}}^{\min} - y_{\mathrm{e}}(\boldsymbol{x}, \boldsymbol{y}^*, \boldsymbol{z}^*)\right) \Phi\left(\frac{y_{\mathrm{e}}^{\min} - y_{\mathrm{e}}(\boldsymbol{x}, \boldsymbol{y}^*, \boldsymbol{z}^*)}{s_{\mathrm{e}}\left(\boldsymbol{x}, \boldsymbol{y}^*, \boldsymbol{z}^*\right)}\right) + s_{\mathrm{e}}\left(\boldsymbol{x}, \boldsymbol{y}^*, \boldsymbol{z}^*\right) \varphi\left(\frac{y_{\mathrm{e}}^{\min} - y_{\mathrm{e}}(\boldsymbol{x}, \boldsymbol{y}^*, \boldsymbol{z}^*)}{s_{\mathrm{e}}\left(\boldsymbol{x}, \boldsymbol{y}^*, \boldsymbol{z}^*\right)}\right) \tag{58}$$

where $y_{\mathrm{c}}^{\min}$ and $y_{\mathrm{e}}^{\min}$ are the minimum values of the responses $\boldsymbol{y}_{\mathrm{c}}$ and $\boldsymbol{y}_{\mathrm{e}}$, respectively, s_{c} and s_{e} are the standard deviation of LF and HF predictions, respectively. If the maximum value of $\mathrm{EI_c}\left(\boldsymbol{x}\right)$ is larger than that of $\mathrm{EI_e}\left(\boldsymbol{x}\right)$, the values of the random variables is determined as the point $\boldsymbol{x}^*$ corresponding to the maximum of $\mathrm{EI_c}\left(\boldsymbol{x}\right)$, and add the new point $(\boldsymbol{x}^*, \boldsymbol{y}^*, \boldsymbol{z}^*)$ to the LF samples. Otherwise, the point $\boldsymbol{x}^*$ corresponding to the maximum of $\mathrm{EI_e}\left(\boldsymbol{x}\right)$ is selected and add the new point $(\boldsymbol{x}^*, \boldsymbol{y}^*, \boldsymbol{z}^*)$ to HF samples.

The flowchart of the proposed approach is shown in Fig. 2.

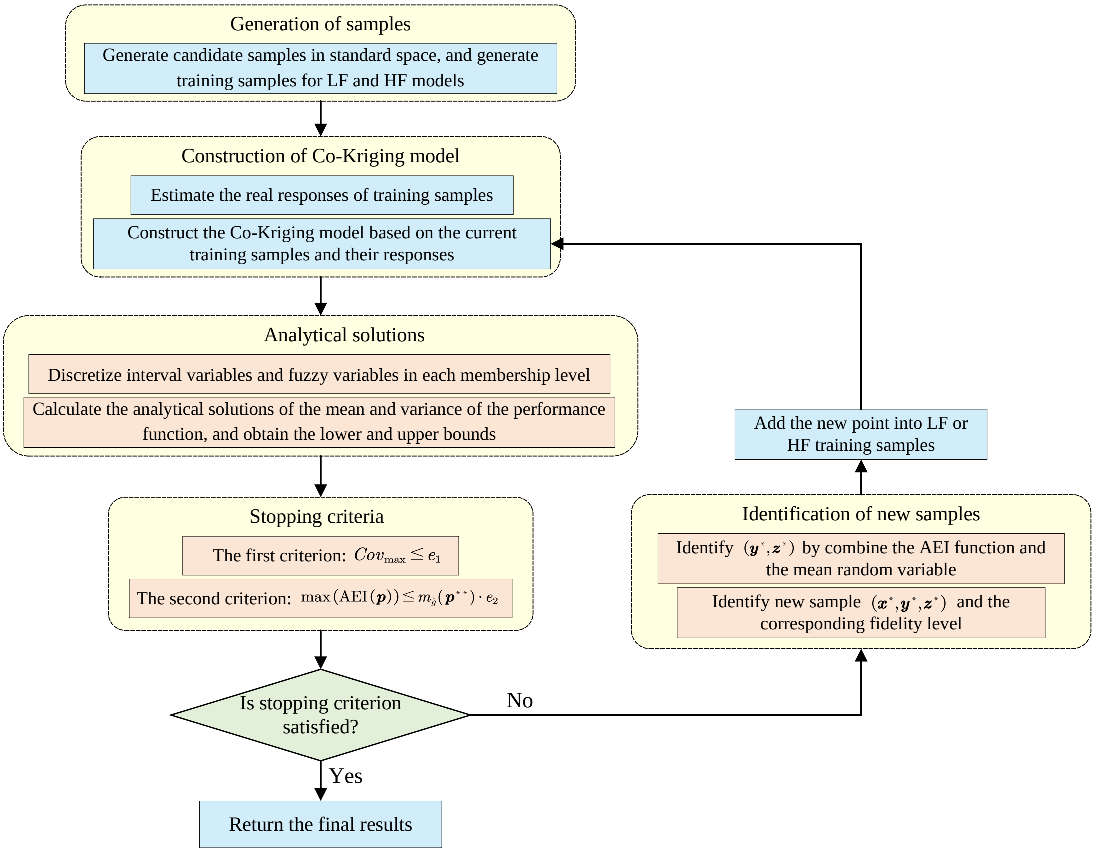

Figure 2: Flowchart of the proposed method

4. Illustrative Examples

In this section, four examples are investigated to validate the efficiency and accuracy of the proposed method, including a mathematical example, a roof truss structure, a planetary transmission gear and a frame structure. In each example, the scaling factor ρ is set to 1, and the candidate sample size N_Ω is set to 10^5. For interval and fuzzy variables, 11 α-cut levels are assigned uniformly to fuzzy variables, and 300 discrete points are generated between the bounds of interval and fuzzy variables at each cut level. The results of the proposed active learning method are obtained over 30 independent runs, and the average results are compared with the reference results obtained by MCS and with the results obtained without active learning (i.e., construct a Co-Kriging model using all the training samples required by the proposed method, and directly estimate the bounds of $u_g(\boldsymbol{y}, \boldsymbol{z})$ and $\sigma_g^2(\boldsymbol{y}, \boldsymbol{z})$).

4.1. Example 1: A mathematical example

The first example is a mathematical problem which is modified from [46]. In this example:

$$
\begin{aligned}
g^h(\boldsymbol{X}, Y, Z) &= \sin\left(\frac{5X_1}{2}\right) - \frac{(X_1 Z + 4)(X_2 - 1)}{20} + Y \\
g^l(\boldsymbol{X}, Y, Z) &= \sin\left(\frac{5X_1}{2}\right) - \frac{(0.9X_1 Z + 4)(0.9X_2 - 1)}{20} + 0.9Y
\end{aligned}
\tag{59}
$$

where $g^h(\cdot)$ and $g^l(\cdot)$ denote the HF and LF models, respectively. In this example, two independent random variables, one interval variable and one fuzzy variable are included. The details of these uncertain variables are listed in Table 1.

In this example, 20 HF samples and 20 LF samples are generated to construct the initial Co-Kriging model. The error threshold e_1 and e_2 are set to 0.005. Fig. 3 shows the lower and upper bounds of the output mean u_g and the output variance σ_g^2 at each membership level. It is observed that the proposed method has a very good performance in estimating the intervals of the output mean u_g and the output variance σ_g^2, while the results without active learning are not accurate enough. In particular, the bounds of σ_g^2 obtained without active learning deviate significantly from the reference. Table 2 summarizes the comparative results obtained by different methods, where $\underline{\varepsilon}(u_g)$ and $\overline{\varepsilon}(u_g)$ are the maximum relative errors of the lower and upper bounds of u_g, $\underline{\varepsilon}\left(\sigma_g^2\right)$ and $\overline{\varepsilon}\left(\sigma_g^2\right)$ are the maximum relative errors of the lower and upper bounds of σ_g^2. It can be seen that the results obtained without active learning have the largest error for the upper bound of σ_g^2, which is 7.90% corresponding to the membership level 0. The maximum relative error of u_g obtained by the proposed method is 0.36% corresponding to the membership level 1, while the maximum relative error of σ_g^2 is 0.44% corresponding to the membership level 1. Compared to MCS, the function calls of the proposed method are greatly reduced, requiring only 32 evaluations of the HF model and 58 evaluations of the LF model. In addition, through kernel density estimation, the PDFs of the output obtained by the three methods at two different points of interval and fuzzy variables are plotted in Fig. 4. It can been seen that the estimated PDFs of the proposed method are almost identical to the reference PDFs, while the PDFs obtained without active learning are less accurate. Thus, the proposed method has prominent performance in terms of efficiency and accuracy.

Table 1: Uncertain variables in Example 1.

Uncertain variables	Distribution types	Parameter 1	Parameter 2
X_1	Normal	1.5	1
X_2	Normal	2.5	1
Y	Interval	2	2.5
Z	Fuzzy	Triangular	(1.5, 2, 2.5)

For the random variable, parameter 1 and 2 are the mean and standard deviation, respectively; for the interval variable, parameter 1 and 2 are the lower and upper bounds, respectively; for the fuzzy variable, parameter 1 and parameter 2 are the type of membership function and the function parameters

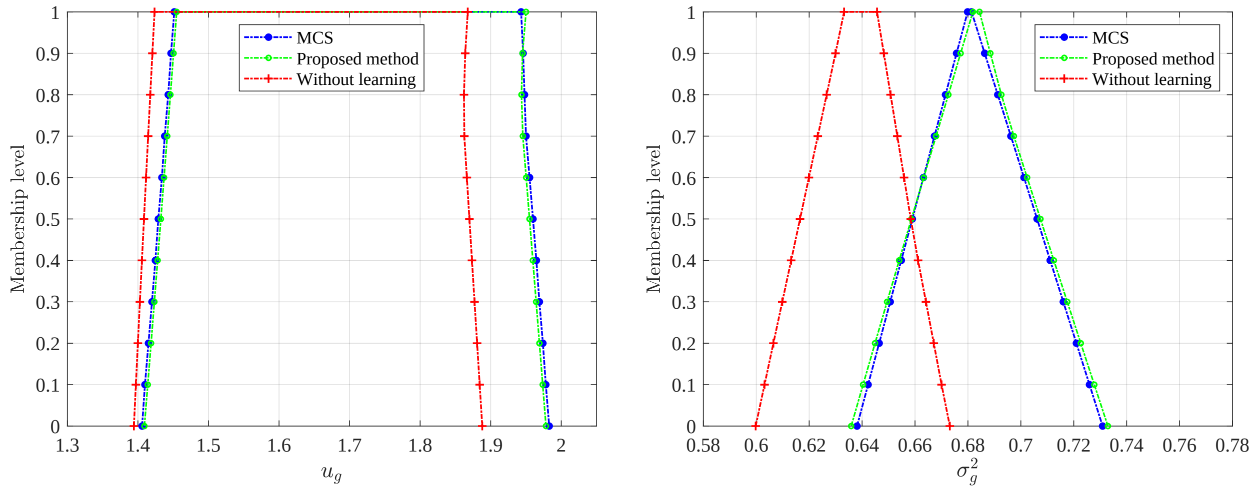

(a) mean

(b) variance

Figure 3: The bounds of the mean u_g and variance σ_g^2 in Example 1

Table 2: Comparative results in Example 1.

Methods	$\underline{\varepsilon}\left(u_g\right)$	$\overline{\varepsilon}\left(u_g\right)$	$\underline{\varepsilon}\left(\sigma_g^2\right)$	$\overline{\varepsilon}\left(\sigma_g^2\right)$	Function costs
MCS	-	-	-	-	$10^5\times$ 300 $\times$11
Proposed method	0.28% ($\alpha = 0.1$)	0.36% ($\alpha = 1$)	0.35% ($\alpha = 0$)	0.44% ($\alpha = 1$)	32HF+58LF
Without learning	1.93% ($\alpha = 1$)	4.79% ($\alpha = 0$)	6.87% ($\alpha = 1$)	7.90% ($\alpha = 0$)	32HF+58LF

4.2. Example 2: A roof truss

As shown in Fig. 5, this example investigates a roof truss structure, which is modified from [47]. For this structure, the bottom boom and the tension bars are steel, while the top boom and the compression bars are reinforced by concrete. Assume that this roof structure is subjected to the uniformly distributed

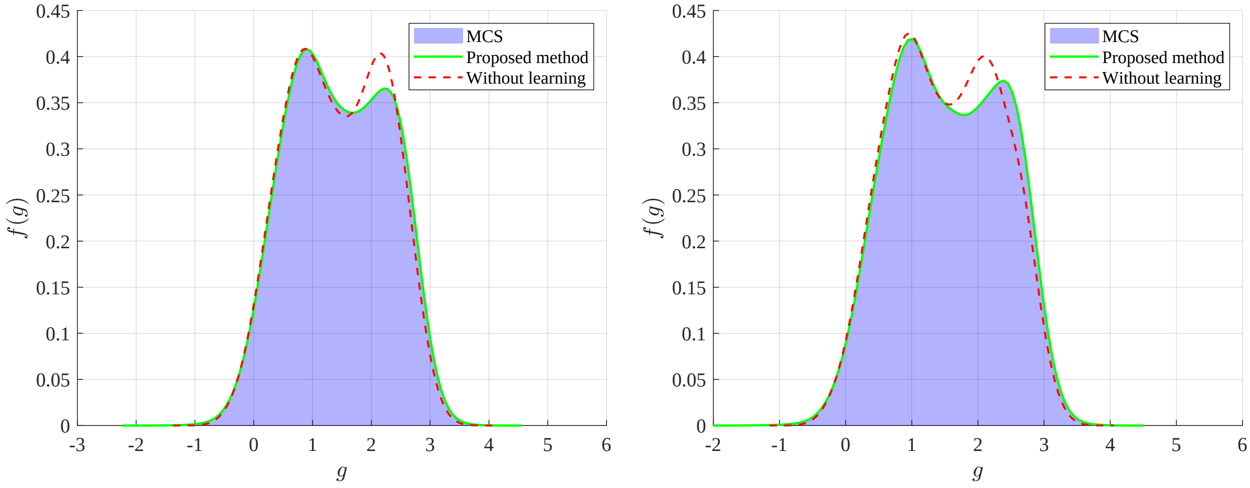

(a) PDFs ($Y = 2$ and $Z = 2$) (b) PDFs ($Y = 2.5$ and $Z = 2$)

Figure 4: The PDFs of the output in Example 1

load q, which can be equivalently transformed to the nodal load $P = ql/4$. We focus on the vertical deflection Δ_{C} at the node C, where the HF and LF models are expressed as follows:

$$\Delta_{\mathrm{C}}^{h} = \frac{ql^2}{2}\left(\frac{3.81}{A_c E_c} + \frac{1.13}{A_s E_s}\right) \tag{60}$$

$$\Delta_{\mathrm{C}}^{l} = \frac{q\left(l+1\right)^2}{2}\left(\frac{3.81}{A_c\left(E_c + 1e7\right)} + \frac{1.13}{A_s\left(E_s + 1e7\right)}\right) \tag{61}$$

where A_S and A_c denote the cross-sectional area of the steel and concrete bars, respectively, E_S and E_c denote their Young's modulus, respectively. Table 3 gives the information of uncertain variables. For the truncated Gaussian distribution, the range values is between positive and negative 3 sigma intervals.

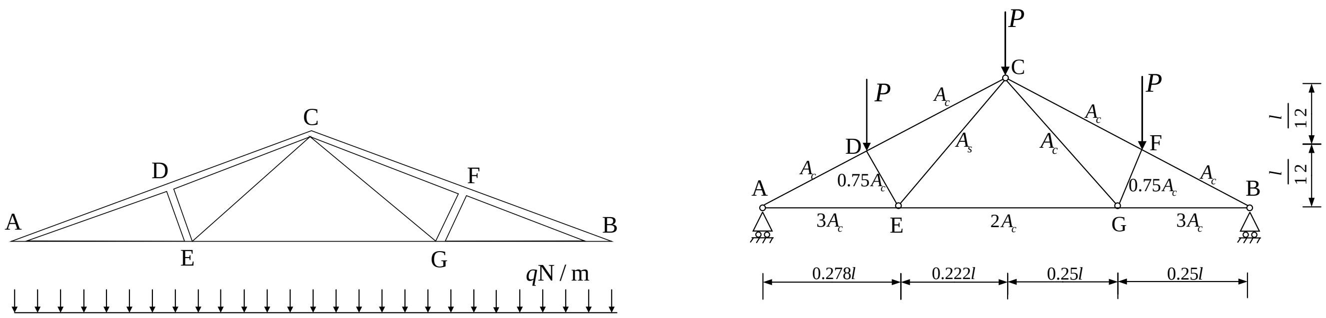

Figure 5: Schematic structural view of the roof truss

Initially, the number of training samples for the HF and LF models is set to 28 and 28, respectively. The error thresholds e_1 and e_2 are set to 0.005 and 0.0001 in this example. Three methods are applied

Table 3: Uncertain variables of the roof truss structure.

Uncertain variables	Distribution types	Parameter 1	Parameter 2
q (N/m)	Truncated Gaussian	20000	1600
l (m)	Truncated Gaussian	12	0.24
E_s (N/m^2)	Truncated Gaussian	1.2×10^{11}	8.4×10^{9}
E_c (N/m^2)	Truncated Gaussian	3×10^{10}	2.4×10^{9}
A_s (m^2)	Interval	9.2×10^{-4}	9.6×10^{-4}
A_c (m^2)	Fuzzy	Triangular	(0.032, 0.034, 0.036)

Parameters 1 and 2 are the same as those in Table 1

to obtain the intervals of the output mean u_g and the output variance σ_g^2 of the vertical deflection Δ_{C}. The bounds of u_g and σ_g^2 are drawn in Fig. 6, Table 4 lists the maximum relative error and the function calls of different methods, and the PDFs estimated by the three methods are also plotted in Fig. 7. It can be seen in Fig. 6 that the lower and upper bounds of u_g and σ_g^2 obtained by the proposed method are almost identical to the reference solutions, while the bounds of σ_g^2 estimated directly without active learning do not agree so well with the reference bounds obtained by MCS. From Table 4, the maximum relative error of the lower and upper bounds of u_g caused by the proposed method are 0.10% and 0.12%, when the membership level is 0.4 and 0.7, respectively. Moreover, the maximum relative error of the bounds of σ_g^2 caused by the proposed method is 0.19%, which is smaller than that caused by the direct estimation without active learning. The function calls of the proposed method are 49 evaluations of HF models and 78 evaluations of LF models, while the function calls of MCS is $10^5 \times 300 \times 11$. In Fig. 7, it is observed that the PDF shapes obtained by the proposed method agree well with the reference. Accordingly, the proposed method can produce more accurate results than direct estimation without active learning, and can obtain the lower and upper bounds of u_g and σ_g^2 with only a few HF samples.

Table 4: Comparative results for the roof truss structure.

Methods	$\underline{\varepsilon}\left(u_g\right)$	$\overline{\varepsilon}\left(u_g\right)$	$\underline{\varepsilon}\left(\sigma_g^2\right)$	$\overline{\varepsilon}\left(\sigma_g^2\right)$	Function costs
MCS	-	-	-	-	$10^5 \times$ 300 $\times 11$
Proposed method	0.10% ($\alpha = 0.4$)	0.12% ($\alpha = 0.7$)	0.19% ($\alpha = 0$)	0.19% ($\alpha = 0$)	49HF+78LF
Without learning	0.15% ($\alpha = 1$)	0.15% ($\alpha = 0.7$)	1.61% ($\alpha = 1$)	1.50% ($\alpha = 0$)	49HF+78LF

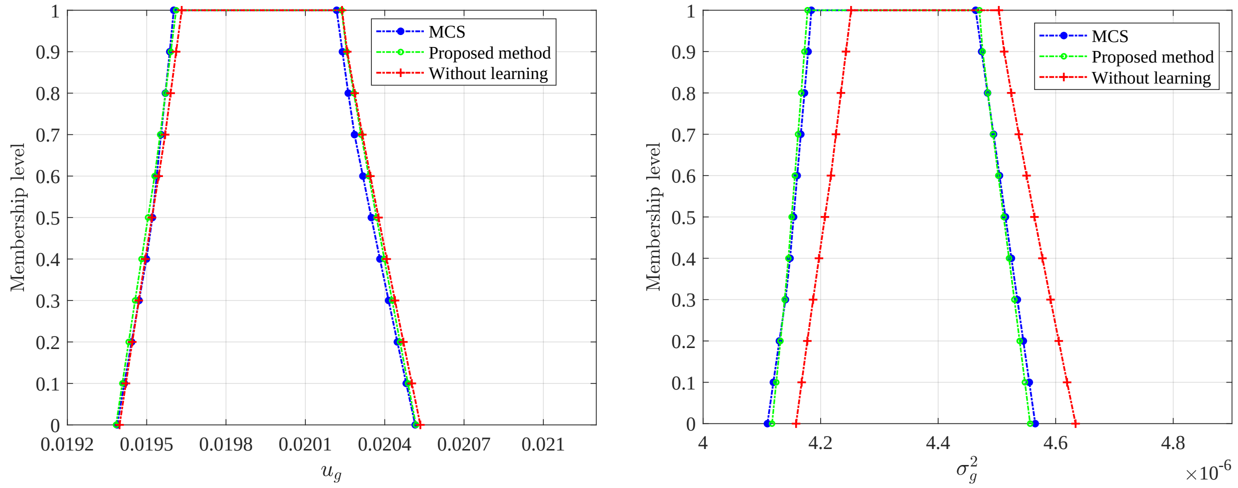

(a) mean (b) variance

Figure 6: The bounds of the mean and variance of the vertical deflection Δ_C

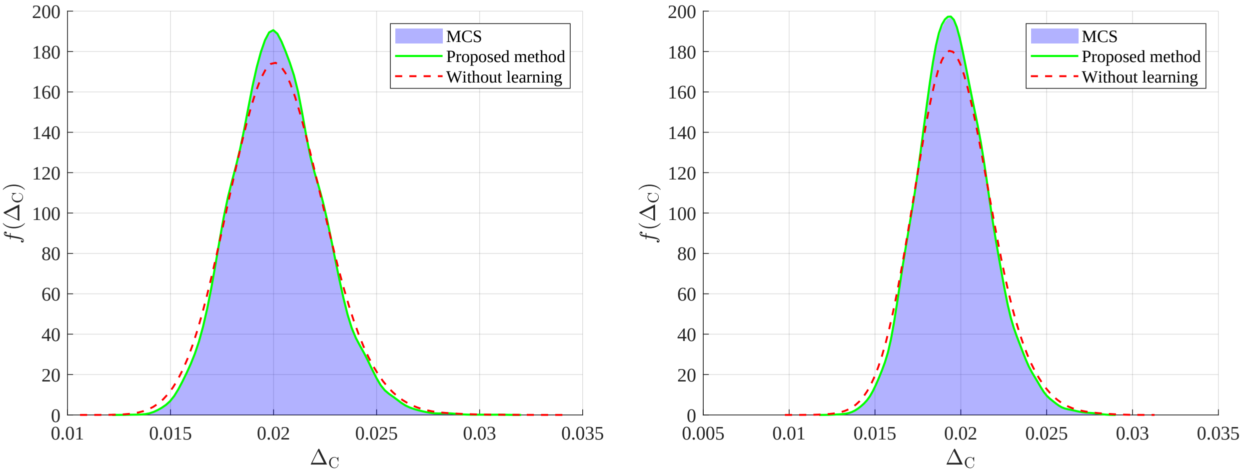

(a) PDFs ($A_s = 9.2 \times 10^{-4}$ and $A_c = 0.034$) (b) PDFs ($A_s = 9.6 \times 10^{-4}$ and $A_c = 0.034$)

Figure 7: The PDFs of the vertical deflection Δ_C

4.3. Example 3: A planetary transmission gear

A planetary transmission gear system, as shown in Fig. 8, is studied to demonstrate the proposed method when dealing with a practical engineering problem. This gear system consists of a ring gear, three planet gears, and a sun gear that serves as the input gear. The pressure angle α_k, module m and tooth width b for all gears are 20 degrees, 1.5mm and 30mm, respectively. The numbers of teeth for the sun gear, the planet gear and the ring gear are 36, 21 and 78, respectively. All gears are made of the same material. The Young's modulus E, the Poisson's ratio υ and the coefficient of friction f are random variables, while the transmitted torque T is a fuzzy variable. Table 5 lists the statistical information of the uncertain variables. For the truncated Gaussian distribution, the range values is between positive and negative 3 sigma intervals. As shown in Fig. 9, the maximum contact stress σ_{H} on the planet gear is the response of interest, which is calculated by the finite element software ABAQUS. For the HF model, the initial and maximum increment sizes are 0.01. For the LF model, the initial and maximum increment sizes are set to 0.05 and 0.1, respectively. The simulation time for each run of the HF model is about 2 hours, while the simulation time for each run of the LF model is about 30 minutes.

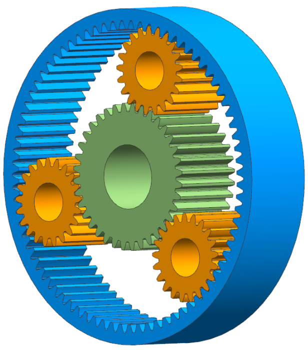

Figure 8: The planetary transmission gear

Table 5: Uncertain variables of the planetary transmission gear.

Uncertain variables	Distribution types	Parameter 1	Parameter 2
E (MPa)	Lognormal	210000	10500
ν	Truncated Gaussian	0.3	0.015
f	Truncated Gaussian	0.05	0.0025
$T(\mathrm{N}\cdot\mathrm{mm})$	Fuzzy	Triangular	$(2.95\times10^5, 3.0\times10^5, 3.05\times10^5)$

Parameters 1 and 2 are the same as those in Table 1

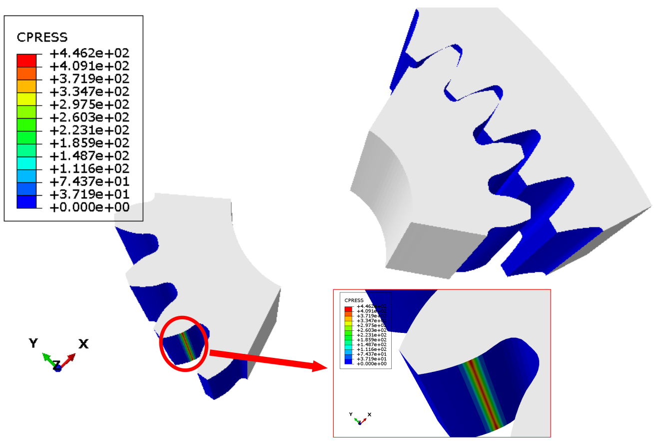

Figure 9: The stress result of planetary transmission gear

To perform MCS as the reference results, 100 HF samples are generated to construct a sparse polynomial chaos expansions (PCE) model with the maximum degree 4 to approximate the true finite element model. 10 HF samples are used as the test set, and the root mean square error (RMSE) is 0.003. In addition, the construction and update of Co-Kriging model are based on the sparse PCE model. In this example, 18 LF and 18 HF samples are chosen to construct the initial Co-Kriging model. The error threshold e_1 and e_2 are 0.002 and 0.0001. The lower and upper bounds of u_g and σ_g^2 of maximum contact stress are shown in Fig. 10. The comparative results of this example are presented in Table 6. The maximum relative errors of u_g and σ_g^2 bounds introduced by the proposed method are 0.01% and 3.44%, respectively, both occurring at the membership level $\alpha = 0$. Without active learning, the maximum relative errors of u_g and σ_g^2 bounds are 0.03% and 40.19%, respectively. In terms of accuracy, the average results of σ_g^2 have larger relative errors than the average results of u_g. 84 evaluations of the HF model and 46 evaluations of the LF model are required by the proposed method, which is fewer than that by MCS. In this example, there are more HF points than LF points, which may be due to the lack of accuracy of the LF finite element model. In Fig. 11, the PDF shapes obtained by different methods are provided. It can be found that compared to the direct estimation without active learning, the proposed method can produce more accurate results of the output variance and the shape of the PDF. Thus, it is demonstrated the efficiency and accuracy of the proposed method for the hybrid uncertainty analysis of structures.

Table 6: Comparative results for the planetary transmission gear.

Methods	$\underline{\varepsilon}(u_g)$	$\overline{\varepsilon}(u_g)$	$\underline{\varepsilon}\left(\sigma_g^2\right)$	$\overline{\varepsilon}\left(\sigma_g^2\right)$	Function costs
MCS	-	-	-	-	$10^5\times$ 300 $\times$11
Proposed method	0.01% ($\alpha = 0$)	0.01% ($\alpha = 0$)	3.44% ($\alpha = 0$)	1.16% ($\alpha = 0$)	84HF+46LF
Without learning	0.03% ($\alpha = 1$)	0.03% ($\alpha = 0.6$)	33.04% ($\alpha = 1$)	40.19% ($\alpha = 0$)	84HF+46LF

4.4. Example 4: A two-bay ten-story frame structure

A two-bay ten-story spatial steel frame structure is considered in this example, which requires the finite element analysis, as shown in Fig. 12. The OpenSees software is employed to model and analyze

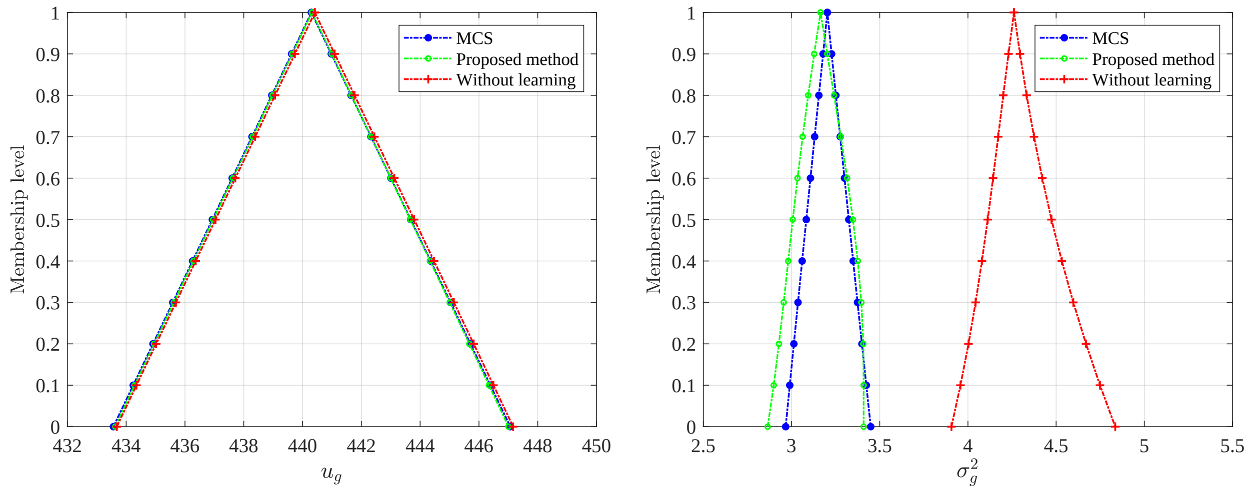

(a) mean (b) variance

Figure 10: The bounds of the mean and variance of the maximum contact stress σ_{H}

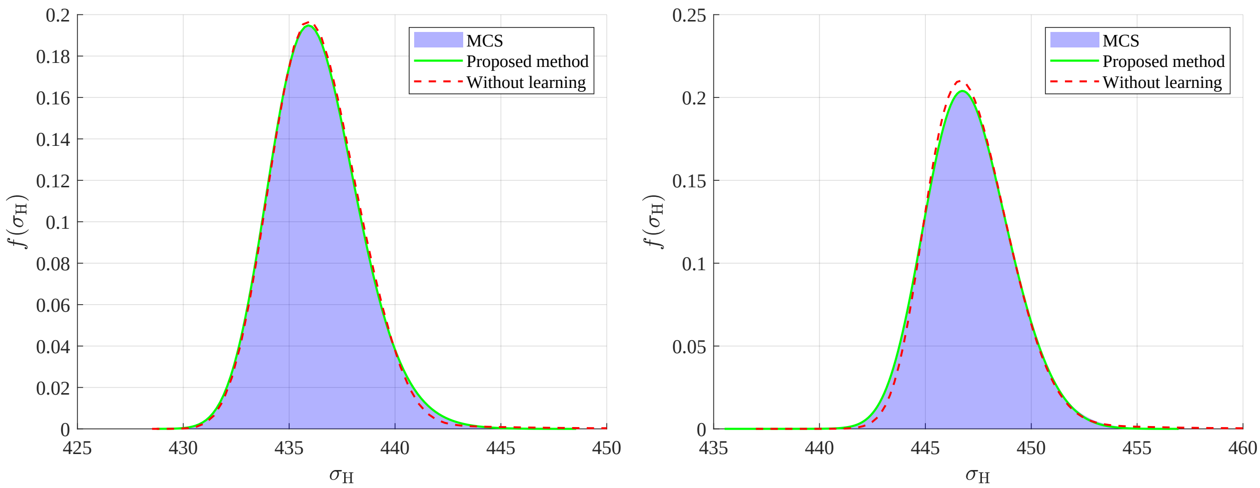

(a) PDFs ($T = 2.97 \times 10^5$) (b) PDFs ($T = 3.05 \times 10^5$)

Figure 11: The PDFs of the maximum contact stress σ_{H}

this frame structure, and the roof drift is adopted as the response of interest, which is symbolized as D_r. In this example, the slab of each floor is supposed to be rigid. The random variables include the Young's modulus of the beams and columns (denoted as E_b and E_c, respectively), the cross-sectional area of the bottom column (denoted as A_{c1}), the cross-sectional area of the remaining columns (denoted as A_{c2}), and seven concentrated loads $F_i\,(i = 1, 2, ..., 7)$. The interval variables consist of two concentrated loads F_8 and F_9. The load F_{10} and the cross-sectional area of the beam are fuzzy variables. Table 7 lists the statistical information of the uncertain variables. For the truncated Gaussian distribution, the range values is between positive and negative 3 sigma intervals. For the LF model, the load F_{10} is discarded.

To save computational time, the reference solution of MCS is performed using the Kriging model, with 270 HF samples used as the training set and 30 HF samples used as the test set. The RMSE of the Kriging model is 0.049.

68 LF and 68 HF training samples are generated to construct the initial Co-Kriging model. The error thresholds e_1 and e_2 are set to 0.005 and 0.0005, respectively. The lower and upper bounds of u_g and σ_g^2 of D_r are shown in Fig. 13. It can be observed that as the membership level increases, the bounds of u_g and σ_g^2 become narrower. Moreover, although the bounds of u_g obtained by the proposed method and the direct estimation without active learning both agree well with the reference bounds, the bounds of σ_g^2 obtained by the proposed method are much more accurate than that obtained without active learning. The maximum relative error of the lower and upper bounds of u_g and σ_g^2 are summarized in Table 8. The maximum relative error of the bounds of u_g caused by the proposed method is 0.48% with the membership level $\alpha = 0$, while the maximum relative error without active learning is 3.83%. The maximum relative error of σ_g^2 of the proposed method is 0.76% when the membership level is 0, while the maximum relative error without active learning is 17.07%. The total number of function calls is 115 evaluations of the HF model and 147 evaluations of the LF model, which is fewer than those required by MCS. When the fuzzy variable takes the value of the membership level of 1, the PDFs of D_r at two different values of the interval variable are drawn in Fig. 14. The results indicate that the proposed method can more accurately estimate the output mean and the output variance, as well as the output PDF. In summary, the proposed method demonstrates a high efficiency in hybrid uncertainty propagation analysis and is also applicable to the engineering problems with multiple epistemic uncertainties.

5. Conclusions

A novel decoupled method based on multi-fidelity active learning is proposed to deal with hybrid uncertainty propagation analysis under random, interval and fuzzy variables. The analytical solutions of the output mean and the output variance are derived based on the Co-Kriging model, where the

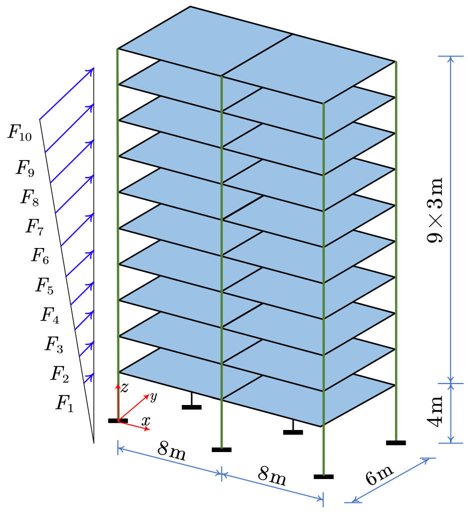

Figure 12: The two-bay ten-story frame structure

Table 7: The statistical information of uncertain variables for the frame structure.

Uncertain variables	Distribution types	Parameter 1	Parameter 2
E_b (MPa)	Truncated Gaussian	3.25×10^4	1.625×10^3
E_c (MPa)	Truncated Gaussian	3.25×10^4	1.625×10^3
A_{c1} (m^2)	Truncated Gaussian	3.6×10^{-1}	1.8×10^{-2}
A_{c2} (m^2)	Truncated Gaussian	1.6×10^{-1}	8×10^{-3}
F_1 (N)	Truncated Gaussian	2.5×10^4	1.25×10^3
F_2 (N)	Truncated Gaussian	2.7×10^4	1.35×10^3
F_3 (N)	Truncated Gaussian	2.9×10^4	1.45×10^3
F_4 (N)	Truncated Gaussian	3.1×10^4	1.55×10^3
F_5 (N)	Truncated Gaussian	3.3×10^4	1.65×10^3
F_6 (N)	Truncated Gaussian	3.5×10^4	1.75×10^3
F_7 (N)	Truncated Gaussian	3.7×10^4	1.85×10^3
F_8 (N)	Interval	3.5×10^4	4.5×10^4
F_9 (N)	Interval	4.0×10^4	5.0×10^4
F_{10} (N)	Fuzzy	Triangular	$(4.5 \times 10^4, 5.0 \times 10^4, 5.5 \times 10^4)$
A_b (m^2)	Fuzzy	Triangular	$(2.0 \times 10^{-1}, 2.4 \times 10^{-1}, 2.8 \times 10^{-1})$

Parameters 1 and 2 are the same as those in Table 1

Table 8: Comparative results for the spatial frame structure.

Methods	$\underline{\varepsilon}(u_g)$	$\overline{\varepsilon}(u_g)$	$\underline{\varepsilon}(\sigma_g^2)$	$\overline{\varepsilon}(\sigma_g^2)$	Function costs
MCS	-	-	-	-	$10^5 \times 300 \times 11$
Proposed method	0.48% ($\alpha = 0$)	0.40% ($\alpha = 0.1$)	0.76% ($\alpha = 0$)	0.37% ($\alpha = 0$)	115HF+147LF
Without learning	3.83% ($\alpha = 0$)	1.44% ($\alpha = 1$)	7.89% ($\alpha = 0$)	17.07% ($\alpha = 0$)	115HF+147LF

variance of the output mean is also derived to measure the uncertainty of the Co-Kriging model. Then, the analytical solutions for the mean and variance of the output mean are employed to enable an active

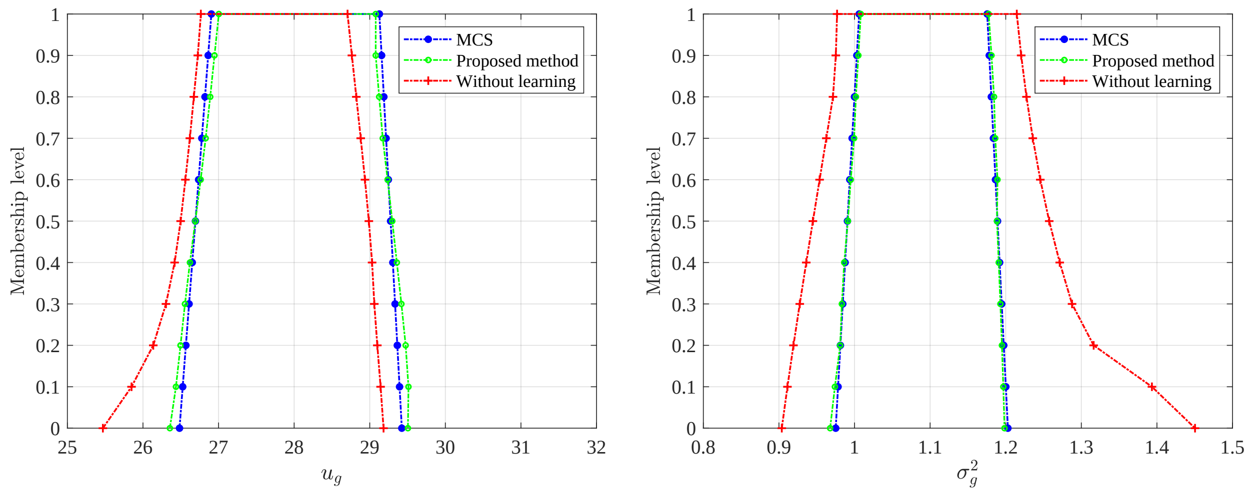

(a) mean (b) variance

Figure 13: The bounds of the mean and variance of the roof drift D_r

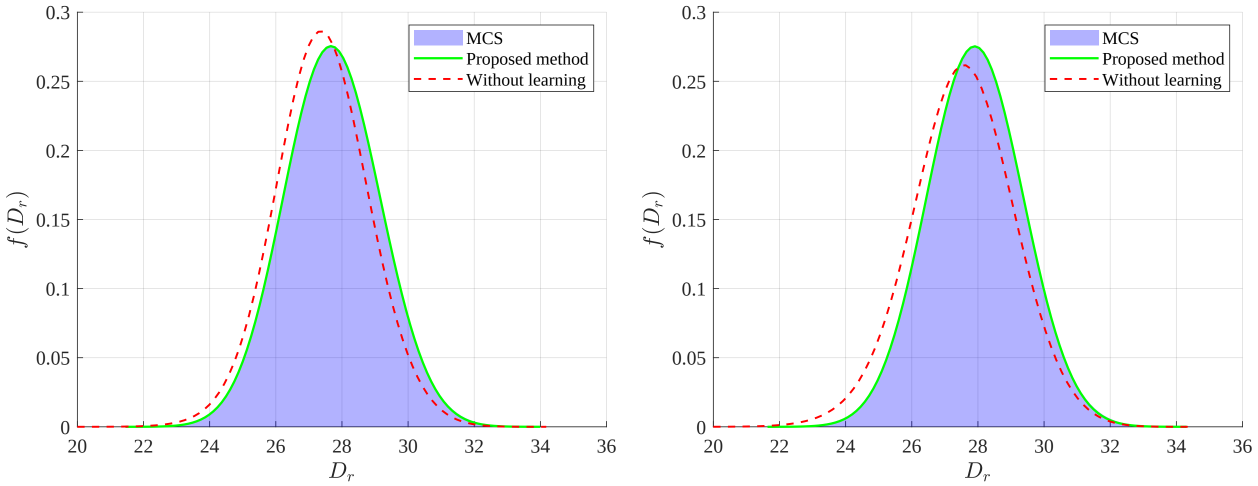

(a) PDFs ($F_8 = 3.6 \times 10^4, F_9 = 4.6 \times 10^4$) (b) PDFs ($F_8 = 3.7 \times 10^4, F_9 = 4.7 \times 10^4$)

Figure 14: The PDFs of the roof drift D_r

learning framework. Finally, the Co-Kriging model update is terminated by considering the coefficient of variation of the output mean and the value of the learning function.

Four examples are used to test the performance of the proposed method. From the comparative results of the four examples, the relative error of the output mean obtained by the proposed method is very small, while the relative error of the output variance is larger but still acceptable, and the proposed method produces more accurate results than the direct estimation without active learning. It is worth noting that this method can avoid the post-processing errors, and can be degraded to handle hybrid uncertainty propagation problems with only two types of uncertain variables. In addition, since the analytical solutions of the output mean and output variance are derived based on Co-Kriging model, this method can deal with efficient hybrid uncertainty propagation for multi-fidelity problems, and the constructed framework can be further incorporated into the sensitivity analysis, RBDO and RDO. For example, in materials science, randomness is present in all materials at some level of resolution [48]. To achieve robust materials design, uncertainty has to be considered, and uncertainty propagation is one of the most important elements. While epistemic uncertainty in model parameters is usually ignored in conventional deterministic approaches [49], the proposed method can deal with hybrid uncertainty propagation for multi-fidelity models.

In the construction of Co-Kriging model, hyper-parameters need to be estimated, where optimization is required. As the dimensionality increases, so does the number of parameters to be estimated, and high-dimensional optimization remains a challenge. It should be noted that our approach is based on Co-Kriging and is not exempt from this limitation. To deal with high-dimensional problems, dimension reduction methods [47, 50] can be incorporated into Co-Kriging to improve efficiency. This is the focus of our future work.

Acknowledgment

This work is supported by the National Natural Science Foundation of China (Grant 52205252), the National Natural Science Foundation of Sichuan Province (Grant 2023NSFSC0876), the Alexander von Humboldt Foundation of Germany, and the China Scholarship Council (CSC).

Conflict of interest statement

The authors declare that they have no conflict of interest.

References

[1] T. H. Lee, J. J. Jung, A sampling technique enhancing accuracy and efficiency of metamodel-based rbdo: Constraint boundary sampling, Comput. Struct. 86 (13-14) (2008) 1463–1476.

[2] Y. Shi, Z. Lu, J. Zhou, E. Zio, A novel time-dependent system constraint boundary sampling technique for solving time-dependent reliability-based design optimization problems, Comput. Methods Appl. Mech. and Eng. 372 (2020) 113342.

[3] B. Do, M. Ohsaki, A random search for discrete robust design optimization of linear-elastic steel frames under interval parametric uncertainty, Comput. Struct. 249 (2021) 106506.

[4] C. van Mierlo, A. Persoons, M. G. Faes, D. Moens, Robust design optimisation under lack-of-knowledge uncertainty, Comput. Struct. 275 (2023) 106910.

[5] M. Shinozuka, Monte carlo solution of structural dynamics, Comput. Struct. 2 (5-6) (1972) 855–874.

[6] S. K. Au, J. L. Beck, Estimation of small failure probabilities in high dimensions by subset simulation, Probab. Eng. Mech. 16 (4) (2001) 263–277.

[7] A. M. Hasofer, N. C. Lind, Exact and invariant second-moment code format, J. Eng. Mech. Div. 100 (1974) 111–121.

[8] Y.-G. Zhao, T. Ono, A general procedure for first/second-order reliabilitymethod (form/sorm), Struct. Saf. 21 (2) (1999) 95–112.

[9] S. Rahman, H. Xu, A univariate dimension-reduction method for multi-dimensional integration in stochastic mechanics, Probab. Eng. Mech. 19 (4) (2004) 393–408.

[10] C. Ding, J. Xu, An improved adaptive bivariate dimension-reduction method for efficient statistical moment and reliability evaluations, Mech. Syst. Signal Process. 149 (2021) 107309.

[11] P. Kersaudy, B. Sudret, N. Varsier, O. Picon, J. Wiart, A new surrogate modeling technique combining kriging and polynomial chaos expansions–application to uncertainty analysis in computational dosimetry, J. Comput. Phys. 286 (2015) 103–117.

[12] B. Sudret, S. Marelli, J. Wiart, Surrogate models for uncertainty quantification: An overview, in: 2017 11th European Conference on Antennas and Propagation, EUCAP, IEEE, 2017, pp. 793–797.

[13] J. C. Helton, D. E. Burmaster, Guest editorial: treatment of aleatory and epistemic uncertainty in performance assessments for complex systems, Reliab. Eng. Syst. Safe. 54 (2-3) (1996) 91–94.

[14] A. Der Kiureghian, O. Ditlevsen, Aleatory or epistemic? does it matter?, Struct. Saf. 31 (2) (2009) 105–112.

[15] R. Y. Rubinstein, D. P. Kroese, Simulation and the Monte Carlo Method, John Wiley & Sons, New Jersey, 2016.

[16] S. S. Rao, L. Berke, Analysis of uncertain structural systems using interval analysis, AIAA J. 35 (4) (1997) 727–735.

[17] S. H. Lee, W. Chen, A comparative study of uncertainty propagation methods for black-box-type problems, Struct. Multidiscip. Optim. 37 (2009) 239–253.

[18] D. Wei, Z. Cui, J. Chen, Uncertainty quantification using polynomial chaos expansion with points of monomial cubature rules, Comput. Struct. 86 (23-24) (2008) 2102–2108.

[19] X. Long, C. Jiang, K. Liu, X. Han, W. Gao, B. Li, An interval analysis method for fatigue crack growth life prediction with uncertainty, Comput. Struct. 210 (2018) 1–11.

[20] J. Liu, H. Liu, C. Jiang, X. Han, Y. F. Hu, et al., A new measurement for structural uncertainty propagation based on pseudo-probability distribution, Appl. Math. Model. 63 (2018) 744–760.

[21] C. Wang, H. G. Matthies, A modified parallelepiped model for non-probabilistic uncertainty quantification and propagation analysis, Comput. Methods Appl. Mech. and Eng. 369 (2020) 113209.

[22] C. Jiang, J. Zheng, X. Han, Probability-interval hybrid uncertainty analysis for structures with both aleatory and epistemic uncertainties: a review, Struct. Multidiscip. Optim. 57 (6) (2018) 2485–2502.

[23] N. Pedroni, E. Zio, E. Ferrario, A. Pasanisi, M. Couplet, Hierarchical propagation of probabilistic and non-probabilistic uncertainty in the parameters of a risk model, Comput. Struct. 126 (2013) 199–213.

[24] C. Wang, H. G. Matthies, Epistemic uncertainty-based reliability analysis for engineering system with hybrid evidence and fuzzy variables, Comput. Methods Appl. Mech. and Eng. 355 (2019) 438–455.

[25] C. Wang, H. G. Matthies, Random model with fuzzy distribution parameters for hybrid uncertainty propagation in engineering systems, Comput. Methods Appl. Mech. and Eng. 359 (2020) 112673.

[26] C. Wang, H. G. Matthies, A comparative study of two interval-random models for hybrid uncertainty propagation analysis, Mech. Syst. Signal Process. 136 (2020) 106531.

[27] C. Dang, P. Wei, M. G. Faes, M. Beer, Bayesian probabilistic propagation of hybrid uncertainties: Estimation of response expectation function, its variable importance and bounds, Comput. Struct. 270 (2022) 106860.

[28] X. Long, D. Mao, C. Jiang, F. Wei, G. Li, Unified uncertainty analysis under probabilistic, evidence, fuzzy and interval uncertainties, Comput. Methods Appl. Mech. and Eng. 355 (2019) 1–26.

[29] Y. Shi, H.-Z. Huang, Y. Liu, M. Beer, Adaptive decoupled robust design optimization, Struct. Saf. 105 (2023) 102378.

[30] Y.-L. Chen, Y. Shi, H.-Z. Huang, D. Sun, M. Beer, Uncertainty analysis of structural output with closed-form expression based on surrogate model, Probab. Eng. Mech. 73 (2023) 103482.

[31] A. I. Forrester, A. Sóbester, A. J. Keane, Multi-fidelity optimization via surrogate modelling, Proc. R. Soc. A 463 (2088) (2007) 3251–3269.

[32] X. Shang, L. Su, H. Fang, B. Zeng, Z. Zhang, An efficient multi-fidelity kriging surrogate model-based method for global sensitivity analysis, Reliab. Eng. Syst. Safe. 229 (2023) 108858.

[33] R. E. Moore, Interval Analysis, Prentice Hall, Englewood Cliffs, 1966.

[34] L. A. Zadeh, Fuzzy sets, Inf. Control 8 (3) (1965) 338–353.

[35] W. Pedrycz, F. Gomide, Fuzzy Systems Engineering: Toward Human-Centric Computing, John Wiley & Sons, New Jersey, 2007.

[36] C. Chen, D. Ran, Y. Yang, H. Hou, C. Peng, Topsis based multi-fidelity co-kriging for multiple response prediction of structures with uncertainties through real-time hybrid simulation, Eng. Struct. 280 (2023) 115734.

[37] L. Mell, V. Rey, F. Schoefs, Two multifidelity kriging-based strategies to control discretization error in reliability analysis exploiting a priori and a posteriori error estimators, Comput. Struct. 274 (2023) 106897.

[38] M. C. Kennedy, A. O'Hagan, Predicting the output from a complex computer code when fast approximations are available, Biometrika 87 (1) (2000) 1–13.

[39] M. Rosenblatt, Remarks on a multivariate transformation, Ann. Math. Statist. 23 (3) (1952) 470–472.

[40] A. Der Kiureghian, P.-L. Liu, Structural reliability under incomplete probability information, J. Eng. Mech. 112 (1) (1986) 85–104.

[41] C. E. Rasmussen, C. K. I. Williams, Gaussian Processes for Machine Learning, Vol. 2, MIT Press, Cambridge, MA, 2006.

[42] P. Wei, X. Zhang, M. Beer, Adaptive experiment design for probabilistic integration, Comput. Methods Appl. Mech. and Eng. 365 (2020) 113035.

[43] C. E. Rasmussen, Z. Ghahramani, Bayesian monte carlo, in: Conference on Neural Information Processing Systems, NeurIPS, 2003, pp. 505–512.

[44] D. Huang, T. T. Allen, W. I. Notz, N. Zeng, et al., Global optimization of stochastic black-box systems via sequential kriging meta-models, J. Glob. Optim. 34 (3) (2006) 441–466.

[45] P. Bratley, B. L. Fox, Algorithm 659: Implementing sobol's quasirandom sequence generator, ACM Trans. Math. Softw. 14 (1) (1988) 88–100.

[46] X. Yang, Y. Liu, Y. Gao, Y. Zhang, Z. Gao, An active learning kriging model for hybrid reliability analysis with both random and interval variables, Struct. Multidiscip. Optim. 51 (2015) 1003–1016.

[47] P. Wang, Z. Lu, Z. Tang, An application of the kriging method in global sensitivity analysis with parameter uncertainty, Appl. Math. Model. 37 (9) (2013) 6543–6555.

[48] M. S. Greene, H. Xu, S. Tang, W. Chen, W. K. Liu, A generalized uncertainty propagation criterion from benchmark studies of microstructured material systems, Comput. Methods Appl. Mech. and Eng. 254 (2013) 271–291.

[49] P. Honarmandi, R. Arróyave, Uncertainty quantification and propagation in computational materials science and simulation-assisted materials design, Integr. Mater. Manuf. Innov. 9 (2020) 103–143.

[50] Z. Song, Z. Liu, H. Zhang, P. Zhu, An improved sufficient dimension reduction-based kriging modeling method for high-dimensional evaluation-expensive problems, Comput. Methods Appl. Mech. and Eng. 418 (2024) 116544.